

# UC Irvine

## UC Irvine Previously Published Works

### Title

Genetic cell targeting uncovers specific neuronal types and distinct subregions in the bed nucleus of the stria terminalis

### Permalink

<https://escholarship.org/uc/item/61n4b44z>

### Journal

The Journal of Comparative Neurology, 524(12)

### ISSN

1550-7149

### Authors

Nguyen, Amanda Q

Dela Cruz, Julie AD

Sun, Yanjun

et al.

### Publication Date

2016-08-15

### DOI

10.1002/cne.23954

Peer reviewed



Published in final edited form as:

*J Comp Neurol.* 2016 August 15; 524(12): 2379–2399. doi:10.1002/cne.23954.

## Genetic cell targeting uncovers specific neuronal types and distinct subregions in the bed nucleus of the stria terminalis

Amanda Q. Nguyen<sup>1,\*</sup>, Julie A.D. Dela Cruz<sup>1,\*</sup>, Yanjun Sun<sup>1,\*</sup>, Todd C. Holmes<sup>4</sup>, and Xiangmin Xu<sup>1,2,3,#</sup>

<sup>1</sup>Department of Anatomy and Neurobiology, School of Medicine, University of California, Irvine, CA 92697-1275

<sup>2</sup>Department of Biomedical Engineering, University of California, Irvine, CA 92697-2715

<sup>3</sup>Department of Microbiology and Molecular Genetics, University of California, Irvine, CA 92697-2715

<sup>4</sup>Department of Physiology and Biophysics, School of Medicine, University of California, Irvine, CA 92697-4560, USA

### Abstract

The bed nucleus of the stria terminalis (BNST) plays an important role in fear, stress, and anxiety. It contains a collection of sub-nuclei delineated by gross cytoarchitecture features; however, there has yet to be a systematic examination of specific BNST neuronal types and their associated neurochemical makeup. The present study focuses on improved characterization of the anterior BNST based on differing molecular and chemical expression aided by mouse genetics. Specific Cre driver lines crossed with a fluorescent reporter line were used for genetic cell targeting and immunochemical staining. Using this new approach, we were able to robustly identify specific excitatory and inhibitory cell types in the BNST. The presence and distribution of excitatory neurons were firmly established; glutamatergic neurons in the anterior BNST accounted for about 14% and 31% of dorsal and ventral BNST cells, respectively. GABAergic neurons expressing different isoforms of glutamic acid decarboxylase were found to have differential sub-regional distributions. Almost no parvalbumin-expressing cells were found in the BNST, while somatostatin-expressing cells and calretinin-expressing cells account for modest proportions of BNST cells. In addition, vasoactive intestinal peptide-expressing axonal plexuses were prominent in the oval and juxtacapsular (jc) subregions. In addition, we discovered that corticotropin-releasing hormone (CRH) expressing cells contain GABAergic and glutamatergic subpopulations. Together, this study reveals new information on excitatory and inhibitory neurons in the BNST, which will facilitate genetic dissection and functional studies of BNST subregions.

#Address all manuscript correspondence to: Dr. Xiangmin Xu, Department of Anatomy and Neurobiology, School of Medicine, University of California, Irvine, CA 92697-1275, Tel: 949 824 0040 Fax: 949 824 8549, xiangmin.xu@uci.edu.

\*These authors contributed equally to this study

### Statement of conflict of interests

All authors disclose no conflict of interests for this work.

## Keywords

transgenic; GABAergic; glutamatergic; immunochemical; BNST; subregions

---

## INTRODUCTION

The bed nucleus of the stria terminalis (BNST) coordinates neuroendocrine, autonomic and somatomotor responses to anxiety and emotional aspects of stressful events (Crestani et al., 2013; Dong and Swanson, 2006; Moga et al., 1989; Walker et al., 2003). This area has received increased attention in light of recent physiological and functional studies (Deisseroth, 2014; Jennings et al., 2013; Johansen, 2013; Kim et al., 2013). Based on gross anatomical and cytoarchitecture features, the BNST can be generally divided into anterior and posterior portions by the presence of anterior commissure (Wood and Swann, 2005). We focused our examination on the anterior BNST for robust identification and delineation of this region. The anterodorsal BNST (adBNST) can be divided into several subregions: the anterolateral (alBNST), the oval (ovBNST) and juxtacapsular (jcBNST) sub-nuclei, as well as the anteromedial (ambBNST) region (Dong et al., 2001; Ju and Swanson, 1989; Ju et al., 1989; Kim et al., 2013; Moga et al., 1989). The ventral BNST also contains sub-nuclei embedded within a relatively undifferentiated region (Ju and Swanson, 1989). The adBNST has been implicated in the expression of affective behaviors, especially to those elicited by stressful stimuli (Dong and Swanson, 2004; Kim et al., 2013). Interestingly, the ovBNST, a subregion of the adBNST, has been found to have an opposing function as compared to the surrounding adBNST regions and has been shown to exert opposite effects on anxious states. The ovBNST activity promotes several anxious behavioral expression while the remaining regions of the BNST exert anxiolytic modulation for the same features (Kim et al., 2013). Additionally, the ventral BNST has been reported to have functionally opposing neuronal types to regulate the ventral tegmental area (VTA) circuits of rewarding and aversive motivational states (Egli and Winder, 2003; Georges and Aston-Jones, 2001; Jennings et al., 2013; Silberman and Winder, 2013). The physiology and function of these BNST subregions or subnuclei are likely determined by specific neuronal constituents and their differential circuit connections. However, the neurochemical makeup of the BNST has not been thoroughly explored, and additional studies are required to understand specific cell types of the BNST (Bota et al., 2012; Larriva-Sahd, 2006; Magableh and Lundy, 2014; Moga et al., 1989).

In the current study, multiple transgenic mouse lines expressing specific molecular and neurochemical markers were used in conjunction with immunochemical staining to identify BNST cell types. Different BNST neuron types were targeted based on their specific molecular and chemical expression using currently available Cre-driver mouse lines. We first addressed the question of how excitatory and inhibitory neurons are distributed in the BNST. Although the BNST cells are believed to be predominantly GABAergic, the excitatory neuronal components of the BNST are poorly understood. Next, given that inhibitory GABAergic neurons have diverse subtypes, we examined and quantified specific inhibitory neuronal subtypes in the BNST. Lastly, due to the fact that corticotropin-releasing hormone (CRH) expressing neurons and cholinergic neurons can be important for modulating BNST

function, we also investigated their distributions and the occurrences of neurochemical colocalization along with other cell types. This study has shed new light on BNST neuronal components and subregions, and will facilitate further studies of specific inhibitory and excitatory neurons in the BNST.

## MATERIAL & METHODS

### Animals

All animals were handled and experiments were conducted in accordance with procedures approved by the Institutional Animal Care and Use Committee at the University of California, Irvine. The animal strains, ages, and number of animals used are detailed in Table 1. The age range of rodents is commonly used for BNST slice electrophysiological experiments is 4–8 weeks (Dabrowska et al., 2013; Egli and Winder, 2003; Hammack et al., 2007; Hazra et al., 2011; Rodriguez-Sierra et al., 2013; Silberman et al., 2013; Turesson et al., 2013). Although we used most animals of 4–6 weeks old for quantitative analysis, we also examined older animals (8–10 weeks) as additional controls. No general differences were found in the distribution patterns and selected chemical staining properties when comparing data collected from the mice of 4–8 weeks versus 8–10 weeks old. We also cited the large database of Allen Institute of Brain Science mouse gene expression (Available from: <http://mouse.brain-map.org/>), which was collected from the mice of 8 weeks old (Lein et al., 2007).

All the mice of either sex were used and maintained in C57BL/6 congenic background. The mice expressing Cre-recombinase (Cre) in specific cell types were obtained from Jackson Laboratory: Camk2a-Cre (stock # 005359), ChAT-IRES-Cre (stock # 006410), CR-IRES-Cre (stock # 010774), CRH-IRES-Cre (stock # 012704), GAD2-IRES-Cre (stock # 010802), PV-IRES-Cre (stock # 012358), SOM-IRES-Cre (stock # 013044), VGLUT2-IRES-Cre (stock # 016963), and VIP-IRES-Cre (stock # 010908). These mice were crossed with a Cre-dependent fluorescent reporter mouse line, Ai9 (Jackson Laboratory stock # 007909; Ai9 transgene: Rosa-CAG-LSL-tdTomato-WPRE, Jackson Laboratory) (Madisen et al., 2010). With this cross, the red fluorescent protein, tdTomato is expressed in the Cre-defined neurons. In a few cases, we crossed Cre lines to the Ai32 reporter mouse line (Jackson Laboratory stock # 012569; Ai32 transgene: Rosa-CAG-LSL-ChR2(H134R)-EYFP-WPRE) (Madisen et al., 2010). The mouse lines of Camk2a-Cre and VGLUT2-Cre were used to target excitatory cell types while GAD2-Cre, PV-Cre, SOM-Cre, CR-Cre and VIP-Cre mice intended to target inhibitory cell types. The GAD67-GFP knock-in hemizygous mice (Tamamaki et al., 2003) maintained in our colony were used to label GAD67+ inhibitory GABAergic neurons. In addition, corticotrophin-releasing hormone (CRH) cells and cholinergic cells expressing choline acetyltransferase (ChAT) were studied using CRH-Cre and ChAT-Cre mouse lines, respectively. The Cre recombinase activity in the Cre lines have been reported as specific and efficient, recapitulating endogenous expression pattern of specific molecules of interests (Taniguchi et al., 2011; Vong et al., 2011). In this study, as described below, we have independently assessed the fidelity of targeting specific cell types using these Cre/transgenic mice.

## Tissue Preparation and Immunochemical Staining

The animals were deeply anesthetized with Euthasol (sodium pentobarbital, 100 mg/kg, i.p.) or isoflurane and perfused transcardially with 5 ml 0.1 M phosphate-buffered saline (PBS; pH 7.3–7.4) and followed by 20 mL PBS containing 4% paraformaldehyde (PFA). The brain was removed from the skull and was postfixed overnight in the same fixative, and then transferred into 30% sucrose in PBS for at least two days. The brain was sectioned at 25  $\mu$ m coronally with a freezing microtome (Leica SM 2010R, Nussloch, Germany). For tissue preparation of CRH staining, CRH-Cre; Ai9 mice received a single intracerebroventricular injection of colchicine (Tocris Bioscience, Bristol, UK, 30  $\mu$ g/0.5  $\mu$ l saline) 24 hours prior to perfusion to enhance CRH peptide localization in neuronal cell bodies (Dabrowska et al., 2013; Sawchenko, 1987).

Conventional fluorescent immunohistochemistry was performed on selected brain sections as previously described (Xu et al., 2006, 2010). The antibodies used for staining are listed in Table 2. Besides fluorescent genetic labeling (tdTomato, GFP), we performed additional single or double immunostaining against selected chemical markers. Free-floating sections were washed 3–5 times with PBS. The sections were incubated in a blocking solution (5% normal donkey serum and 0.05–0.1% Triton X in PBS) for 2 hours at room temperature. Sections were then incubated with one or two primary antibodies in the blocking solution at the appropriate dilution for 36 hours at 4°C. Afterwards, the sections were washed thoroughly with PBS, and then incubated with one or two appropriate secondary antibodies with differential fluorophores (i.e., Alexa Fluor 488, 594, 647) (Jackson ImmunoResearch, West Grove, PA) in the blocking solution for 2 hours at room temperature. Next, the sections were counterstained with DAPI (4',6-diamidino-2-phenylindole) for better visualization of cortical and subcortical structures. The sections were washed, wet-mounted and coverslipped with mounting medium Vectashield (H-1000, Vector, Burlingame, CA).

## Antibody characterization and specificity

Most of the primary antibodies used in our staining experiments are commercially available from major companies. Please see our previous publications (Xu et al., 2006 and 2010) for detailed information regarding the GABA, PV, CR, SOM and VIP antibody characterization and specificity. Based on technical information from Santa Cruz Biotechnology, the calcium/calmodulin-dependent protein kinase II (CaMKII) antibody (M-176) is a rabbit polyclonal antibody raised against amino acids 303–478 mapped at the C-terminus of CaMKII $\alpha$  of mouse origin, and it is recommended for detection of CaMKII $\alpha$ , CaMKII $\beta$ , CaMKII $\gamma$  and CaMKII $\delta$  subunits of mouse, rat and human origin. The CaMKII antibody specificity has been confirmed with Western blot and immunochemical analysis. The corticotrophin-releasing hormone (CRH) antibody is a rabbit polyclonal antibody made non-commercially at the Salk Institute of Biological Studies (La Jolla, CA), provided to us as a gift from Dr. Paul Sawchenko. The antibody was produced in rabbit using human/rat CRH coupled to human alpha-globulins via bisdiazotized benzidines as immunogen, and was thoroughly characterized and extensively published (Chen et al., 2001; Sawchenko, 1987; Swanson et al., 1983). The CRH antibody has been further validated using CRH-null mice (Chen et al., 2015).

## Image Acquisition and Data Quantification

For cell counting and quantification of genetically labeled and immunolabeled neurons, sections were examined and digitized through a 20x objective with a confocal microscope system (LSM 700, Carl Zeiss Microscopy, Nussloch, Germany) and its related software. For visualization of some sections, we also used an epi-fluorescent Olympus BX61 microscope equipped with a 10X objective and a high-sensitive CCD camera (Hamamatsu Photonics, Tokyo, Japan) using the Metamorph image acquisition software (Molecular Devices, Sunnyvale, CA). Analysis of colocalization of genetic labels and chemical markers was performed using maximum projection images from confocal stacks of optical sections (z thickness of about 10  $\mu\text{m}$ ) to ensure accurate identification of double labeled cells. Quantification was based on digital images using Photoshop CS4 with the manual counting tool. We distinguished and separately measured the dorsal and ventral BNST neurons with robust labeling of cell bodies.

To examine the fidelity of genetic labels and Cre expression in the mouse lines (see the Results for seven different mouse lines), the overall percentages of Cre<sup>+</sup> cells that stain immunohistochemically, and immunohistochemically stained cells that express Cre were measured. Neuronal profile counts from dorsal and ventral BNST were pooled from a total of 3 sections from two different mice of each mouse line for these analysis. Given the lower sensitivity of immunostaining detection than genetic labels in general, we had to ensure the analysis accuracy by examining neuronal profiles in small regions with higher power confocal microscopy. Despite unbiased selections, this led to a trade-off of sampling relatively small numbers of neurons for the analysis.

As summarized in Table 3, the cell density was measured by comparing the total number of specific neuronal types to the defined area sizes of either the dorsal or ventral regions of the BNST sections from 4–6 mice each. We measured every neuronal profile through the region of interest in representative sections. Given the genetic labeling of sparse versus dense populations in different mouse lines, and evenly and unevenly distributed profiles in BNST subregions, we reason that the non-stereological but complete counting method is appropriate for this work. The spatial distribution and regional specificity, the overlap percentages of marker expression, and marker-positive cell densities were assayed. The overall NeuN positive counts were used to estimate the total number of neurons in the region of interest. The final cell counts were corrected using the Abercrombie method, i.e., the ratio of the “real” number to the observed number is  $T/(T+h)$ , where  $T$  = section thickness and  $h$  = the mean diameter of the nuclei of cells along the axis perpendicular to the cutting plane of the section (Guillery, 2002). The  $T$  in our study was 25  $\mu\text{m}$ . In this study, we measured the average  $h$  in the x-y plane for different cell types in both dorsal and ventral BNST, and then used this information for adjusting cell count measurements accordingly. The DAPI-stained nuclear sizes were measured from confocal images of typical coronal sections (two sections from 2 different mice) at the anterior-posterior (AP) level of between 0.1 mm and 0.2 mm. For NeuN immunopositive cells, their average  $h$  was  $8.95 \pm 1.04$  (mean  $\pm$  SD)  $\mu\text{m}$  and  $9.7 \pm 0.92$   $\mu\text{m}$  for dorsal and ventral BNST (measured from 110 cells each), respectively. The average  $h$  of CRH-Cre; Ai9 cells was  $9.06 \pm 1.01$   $\mu\text{m}$  and  $9.14 \pm 1.06$   $\mu\text{m}$ , for dorsal and ventral BNST (measured from 79 and 67 cells each), respectively. The average  $h$  of ChAT-

Cre; Ai9 cells was  $9.06 \pm 1.2 \mu\text{m}$  and  $9.94 \pm 1.75 \mu\text{m}$ , for dorsal and ventral BNST (measured from 10 and 20 cells each, due to sparse labeling), respectively. For Camk2a-Cre; Ai9 cells, their average h was  $8.28 \pm 0.89 \mu\text{m}$  and  $7.35 \pm 1.15 \mu\text{m}$  for dorsal and ventral BNST (measured from 110 and 43 cells), respectively. The average h of VGLUT2-Cre; Ai9 cells was  $8.61 \pm 1.4 \mu\text{m}$  and  $7.2 \pm 1.52 \mu\text{m}$ , for dorsal and ventral BNST (measured from 3 and 22 cells each), respectively. For EAAC+ cells, their average h was  $9.16 \pm 0.85 \mu\text{m}$  and  $9.06 \pm 0.99 \mu\text{m}$  for dorsal and ventral BNST (measured from 70 and 57 cells), respectively. For GAD67-GFP cells, their average h was  $9.55 \pm 0.99 \mu\text{m}$  and  $9.66 \pm 1.04 \mu\text{m}$  for dorsal and ventral BNST (measured from 134 and 37 cells), respectively. GAD2-Cre; Ai9 cells had similar sizes, and their average h was  $9.63 \pm 0.81 \mu\text{m}$  and  $9.61 \pm 0.81 \mu\text{m}$  for dorsal and ventral BNST (measured from 196 and 35 cells), respectively. The average h of CR-Cre; Ai9 cells was  $8.38 \pm 0.9 \mu\text{m}$  and  $8.88 \pm 1.4 \mu\text{m}$ , for dorsal and ventral BNST (measured from 57 and 18 cells each), respectively. The average h of SOM-Cre; Ai9 cells was  $10.33 \pm 0.98 \mu\text{m}$  and  $9.96 \pm 1.11 \mu\text{m}$ , for dorsal and ventral BNST (measured from 102 and 32 cells each), respectively. The average h of VIP-Cre; Ai9 cells was  $7.94 \pm 1.02 \mu\text{m}$  for dorsal BNST (measured from 3 cells, due to little or very sparse neuronal cell body labeling).

### Statistical comparisons

Unless specified otherwise, the data were reported as mean  $\pm$  SE with pooled measurements from representative sections of 4–6 mice (e.g., see Table 3). Differential expression of neurochemical markers between dorsal and ventral BNST were examined. Statistical comparisons of the measurements across groups are made using Kruskal–Wallis test (nonparametric one-way ANOVA) and the Mann–Whitney U test for group comparisons with  $p < 0.05$  considered as significant.

## RESULTS

Specific neuronal types were examined aided by genetic targeting in the adBNST and ventral BNST through the use of multiple transgenic mouse lines. The structures of particular interest are the subregions in the adBNST, including ovBNST, jcBNST, alBNST and amBNST, as well as anterior ventral BNST (the current study refers to it as the vBNST). Although previous studies used different species to study the neuronal populations in the BNST (for review, see (Bota et al., 2012)), we chose to focus our study to the mouse because this species has emerged as an increasingly important model for more recent cortical circuit studies. In addition, the mouse species allows us to better define and delineate specific neuron types using mouse genetics, which can enable us to overcome technical limitations such as low sensitivity/specificity using conventional antibody immunostaining or *in situ* hybridization.

### Transgenic expression and specific chemical markers

First, we established the Cre/transgenic expression in our mouse lines as reasonable surrogates of cell-type specific chemical markers in the BNST. Although these mouse lines have been characterized and validated in the past studies in other brain areas, the Cre expression fidelity in the BNST region has not been previously examined. We quantified the specificity of the Cre expression by measuring Cre+ cells that stain immunohistochemically,

and the efficiency of the Cre expression by measuring the percentage of immunohistochemically stained cells that express Cre. We found that GAD67 label in the GAD67-GFP mouse and GAD2-Cre expression in the GAD2-Cre; Ai9 mouse show good correspondence to GABA immunoreactivity. As illustrated in Figure 1 A–B, based on the measurements from GAD67-GFP mouse sections (see the Methods), 98% GAD67-GFP cells (125/128) in the dorsal BNST were GABA+, and 96% of GABA immunopositive cells (125/130) were GAD67-GFP positive. In the ventral BNST of GAD67-GFP mice, 89% GAD67-GFP cells (55/62) were GABA+, and 86% GABA immunopositive cells (55/64) were GAD67-GFP positive. In the GAD2-Cre; Ai9 dorsal BNST (Figure 1C), 98% of GAD2-Cre; Ai9 cells (127 out of 130 cells) were GABA immunopositive while 90% of GABA immunopositive cells (127/141) showed GAD2-Cre expression (tdTomato expression). However, in the ventral BNST of GAD2-Cre; Ai9 mice, the colocalization rates were lower, as 80% of GAD2-Cre; Ai9 cells (51 out of 64 cells) were GABA immunopositive and particularly 43% of GABA immunopositive cells (51/119) showed GAD2-Cre expression.

Camk2a-Cre expression in Camk2a-Cre; Ai9 mice displays good correspondence to CaMKII immunoreactivity (Figure 1D). In the Camk2a-Cre; Ai9 dorsal BNST, 99% of Camk2a-Cre; Ai9 cells (143/144) are CaMKII immunopositive while 85% of CaMKII immunopositive cells (143/168) showed CaMKII-Cre expression. In the ventral BNST, Camk2a-Cre; Ai9 cells showed high specificity with 96% of the cells immunopositive for CaMKII (49/51), but only 43% of CaMKII immunopositive cells were detected for Camk2a-Cre; Ai9 expression.

While SOM-Cre, VIP-Cre and CRH-Cre appeared to have correspondence to their respective immunoreactivity, CR-Cre did not have robust colocalization with CR immunoreactivity (Figure 2). For dorsal and ventral BNST neurons pooled from selected sections, 25 of 98 SOM-Cre; Ai32 cell bodies are determined to be SOM immunopositive (Figure 2A). But many others (40) had SOM immunoreactivity above neuropil, and when we included them as SOM-positive cells, about 80% of SOM-Cre; Ai32 cells were positive for SOM. The tdTomato expression in dense axonal plexuses of VIP-Cre; Ai9 dorsal BNST was verified by VIP immunoreactivity (Figure 2C). In CRH-Cre; Ai9 mouse BNST, 17 of 52 CRH-Cre; Ai9 cells were determined to be clearly CRH immunopositive in terms of cell body staining. When we included CRH-Cre; Ai9 cells having CRH immunoreactivity above neuropil, about 94% of CRH-Cre; Ai9 cells examined (105/112) were positive for CRH. In contrast, tdTomato expression in the CR-Cre; Ai9 mouse BNST lacked robust colocalization with CR immunoreactivity (Figure 2D). For selected BNST slices, only 5 of 105 CR-Cre; Ai9 cells were determined to be CR immunopositive; only 5 out of 50 CR immunopositive cells expressed tdTomato. Thus, the CR-Cre results should be cautiously interpreted (see below).

In addition, the gene/Cre expression in our mouse lines visualized through GFP or tdTomato (below) are consistent with *in situ* hybridization image data (available at the Allen Mouse Brain Atlas, <http://mouse.brain-map.org>), which corresponds to the markers of Camk2a, VGLUT2, GAD1, GAD2, PV, SOM, VIP, ChAT and CRH (Figure 3). Except CR-Cre, the preceding evidence (see the Discussion below) largely overcomes the concern about

transient Cre expression during the development, which may lead to interpretation issues when examining genetically labeled neurons by crossing Cre and reporter lines.

### Excitatory cells in the BNST

The presence of inhibitory neurons in the BNST is well documented, but the existence and distribution of excitatory neurons in the BNST is much less understood. Previous *in situ* hybridization for vesicular glutamate transporter (VGLUT) and glutamic acid decarboxylase (GAD) has shown numerous GAD-synthesizing neurons and a lack of VGLUT-synthesizing neurons in rat BNST (Larriva-Sahd, 2006). In comparison, a recent study using VGLUT2-IRES-Cre and VGAT-IRES-Cre mouse lines targeting glutamatergic versus GABAergic neurons in ventral BNST indicated the existence of both excitatory and inhibitory cell types in a different BNST region (Jennings et al., 2013).

The current study has established a prominent existence of excitatory glutamatergic neurons in both adBNST and vBNST through genetic targeting and combined immunochemical characterization. Because the BNST is considered as a part of the cerebral nuclei, an examination was started with the excitatory neuronal distribution in the BNST aided by the use of *Camk2a*-Cre; *Ai9* mice (Figure 4). Calcium/calmodulin-dependent protein kinase type II alpha (CaMKII $\alpha$ ), from the gene *camk2a*, is a well-known marker for excitatory neurons distributed in the cerebral cortex. We compared the numbers of CaMKII $\alpha$ -expressing neurons to the overall NeuN positive counts. The expression of CaMKII $\alpha$  was found in about 15% of the total neurons with a density of  $25.04 \pm 2.09$  cells/mm<sup>2</sup> in the adBNST. The majority of CaMKII $\alpha$ -expressing cells were distributed near the lining of the internal capsule, the ovBNST and particularly concentrated in the jcBNST (Figure 4A, B). In addition, a less number of CaMKII $\alpha$  cells were found in the amBNST (Figure 4B). In the vBNST, CaMKII $\alpha$ -expressing cells comprised about 8.6% of the total population with a density of  $12.02 \pm 1.28$  cells/mm<sup>2</sup>, and they were found mainly near the anterior commissure (Figure 4C). Furthermore, VGLUT2-expressing neurons were examined in the BNST with VGLUT2-Cre; *Ai9* mice (Figure 5). VGLUT2 is another excitatory neuronal marker that is mainly expressed in the subcortical regions. Compared to CaMKII $\alpha$ -expressing cells, about 0.39% of the neurons in the adBNST (density of  $0.65 \pm 0.11$  cells/mm<sup>2</sup>) were found to be VGLUT2+ (Figure 5B). The vBNST contained a sparse amount of labeled VGLUT2+ cells, making up 0.93% of the total cells (density:  $1.31 \pm 0.24$  cells/mm<sup>2</sup>) (Figure 5C). The small number of VGLUT2-expressing cells in dorsal BNST was also supported by *in situ* hybridization visualization of VGLUT2 in the BNST (Figure 3B).

Considering that these different excitatory neuronal markers appear to label specific subsets of glutamatergic neurons, an alternative strategy was used to examine the overall glutamatergic BNST cells by immunochemical staining against excitatory amino acid transporter type 1 (EAAC1). The EAAC1 staining robustly labels neurons, but not glial cells as confirmed by NeuN staining (not shown). GABA is synthesized in GABAergic neurons by the decarboxylation of glutamate catalyzed by the enzyme glutamic acid decarboxylase (GAD). Two isoforms of this enzyme are known, which are referred to as GAD65 and GAD67. These isoforms are encoded by two distinct genes, GAD2 and GAD1, respectively. Due to the fact that GABAergic neurons show EAAC1 staining (Conti et al., 1998; Sun et

al., 2014), EAAC1-labeling was performed in sections of cross-bred mice of GAD2-Cre; Ai9/GAD67-GFP. Glutamatergic neurons were identified as EAAC1+ and GAD- (Figure 6). In Figure 6, GAD1 (GAD67) expressing neurons were labeled with GFP (Figure 6C, H), while GAD2 (GAD65) expressing neurons were labeled with tdTomato (Figure 6D, I). The excitatory glutamatergic neurons (EAAC1+/GAD- neurons) were distributed throughout the adBNST and vBNST, representing a major subpopulation of BNST cells. The EAAC1+/GAD- neurons were more abundant in the vBNST, as opposed to the adBNST ( $p = 0.01$ ) (Figures 6A and F, Table 3), comprising approximately 14% of the total neurons in the adBNST and 29% of the total neurons in the vBNST with densities of  $23.01 \pm 2.22$  cells/mm<sup>2</sup> and  $40.36 \pm 4.76$  cells/mm<sup>2</sup>, respectively.

### Inhibitory cells in the BNST

Although inhibitory GABAergic neurons in the BNST have been characterized in morphology and electrophysiology (Hammack et al., 2007; Hazra et al., 2011; Larriva-Sahd, 2004, 2006; McDonald, 1983; Rodriguez-Sierra et al., 2013), the neurochemical compositions of different types of inhibitory neurons have been largely unknown. Based on quantitative examination using cross-bred mice of GAD2-Cre; Ai9/GAD67-GFP, we found that GABAergic neurons determined by GAD1 and/or GAD2 expression account for approximately 66% of the adBNST cells and 32% of the vBNST cells, respectively (Figure 7; Table 3). Because GAD1 and GAD2 are known to present in most of the GABAergic neurons in the brain, the co-localization rates of GAD1/GAD2 and GAD2/GAD1 in concentrated portions of adBNST were similar,  $87\% \pm 1.7\%$  and  $87.2\% \pm 3\%$ , respectively. In contrast, the vBNST contained overall lower GAD1/GAD2 and GAD2/GAD1 colocalization at  $58.9\% \pm 6.9\%$  and  $73.6\% \pm 7.4\%$  ( $p = 0.008$ ), respectively (Figure 6).

GAD1+ cells (via GAD67-GFP labeling) in the adBNST comprised approximately 66% of the total neuronal population (density:  $109.07 \pm 1.88$  cells/mm<sup>2</sup>). GAD1+ cells were found to be distributed throughout the adBNST, and are concentrated near the ovBNST, jcBNST and alBNST, while a smaller number of GAD1+ cells are found in the ambBNST (Figure 7A and B). In the vBNST, GAD1+ comprised approximately 28% of the cells (density:  $39.67 \pm 3.75$  cells/mm<sup>2</sup>) and were scattered in close vicinity to the anterior commissure and lower portions of ventral BNST (Figure 1B; Figure 6F and 7A). GAD2+ cells (via GAD2-Cre; Ai9 labeling) in the adBNST comprised approximately 53% of the total neuronal population (density:  $92.25 \pm 8.93$  cells/mm<sup>2</sup>). Similar to GAD1+ cells, GAD2+ cells was found to be more prevalent in the lateral portion of the adBNST than the ambBNST (Figure 7C, D). In the vBNST, GAD2+ comprised approximately 18% of the total cells (density:  $25.66 \pm 1.29$  cells/mm<sup>2</sup>) (Figure 6F and 7C). Whereas no significant difference was found between GAD1+ and GAD2+ cell densities in the adBNST region, GAD1+ cells was found to have greater density than GAD2+ cells ( $p = 0.03$ ) in the vBNST.

Interestingly, dense GAD2+ cells were clearly prominent in the small region corresponding to jcBNST (Figure 7C, D). This aspect of GAD2 expression in adBNST can be used to help with delineation of the jcBNST. In addition, strong red fluorescent expression in GAD2-Cre; Ai9 mouse sections in the lateral region outside vBNST and dense GAD1+ cells in the

medial region close to the medial preoptic area in the GAD-GFP mouse sections may provide gross cytoarchitecture cues for delineating the border for the vBNST (Figure 7A, C).

Typical interneuronal makers (Xu et al., 2006, 2010) were used to further examine different sub-types of GABAergic cells. Parvalbumin (PV), somatostatin (SOM), calretinin (CR) and vasoactive intestinal peptide (VIP) expression were examined in the sections of PV-Cre; Ai9, SOM-Cre; Ai9, CR-Cre; Ai9 and VIP-Cre; Ai9 mice. Although PV+ neurons are considered the most numerous in the cortex, the neurons appeared rare and largely absent in both the dorsal and ventral BNST. Quantitative analysis showed PV+ neurons in both areas contained less than ~0.4% of their total neuronal population (Figure 8A, B; density, adBNST:  $0.21 \pm 0.13$  cells/mm<sup>2</sup>; density, vBNST:  $0.44 \pm 0.31$  cells/mm<sup>2</sup>). SOM+ cells appeared abundant in the lateral region of the adBNST, comprising about 17% of adBNST neurons (Figure 8C; density:  $27.93 \pm 0.85$  cells/mm<sup>2</sup>). SOM+ cells were fewer in the vBNST, populating about 4.4% of the total neurons (Figure 8D; density:  $6.10 \pm 0.95$  cells/mm<sup>2</sup>). Putative CR+ cells in the adBNST comprised about 10% of the total neurons in the adBNST (density:  $16.94 \pm 2.53$  cells/mm<sup>2</sup>) and were found primarily in the ovBNST (Figure 8E). In the vBNST, putative CR+ cells comprised of about 3.6% of the total neurons in the region (density:  $4.96 \pm 0.83$  cells/mm<sup>2</sup>) (Figure 8F). In addition, VIP+ neurons were scarce in either the adBNST or the vBNST (Figure 9), as these neurons populated less than 0.5% of the entire region. However, VIP+ axonal plexuses, revealed by either genetic labeling or VIP immunostaining (data not shown), were found to be abundant in the ovBNST and jcBNST. Thus, VIP expression can be particularly useful in facilitating the BNST sub-regional delineation.

### Other cell types in the BNST

Corticotropin-releasing hormone (CRH) expressing neurons are known to be important for BNST function, but have not been thoroughly investigated. In order to remedy this fact, CRH-Cre; Ai9 mice were used to examine the CRH distributions and to address their colocalization with GABAergic and glutamatergic cells in the BNST. A number of CRH-expressing neurons were found to be distributed throughout the adBNST and vBNST (Figure 10). In the adBNST, CRH+ cells comprised approximately 8% of total neurons (density:  $13.74 \pm 1.56$  cells/mm<sup>2</sup>). In the vBNST, CRH+ neurons comprised of about 13% of the total neurons (density: of  $18.52 \pm 1.44$  cells/mm<sup>2</sup>). CRH+ neurons were found almost exclusively in the BNST but not in its surrounding regions. Previous immunostaining evidence indicates that CRH+ cells are found to be inhibitory neurons in rat hippocampus and a portion of the rat BNST (Chen et al., 2001; Dabrowska et al., 2013; Yan et al., 1998), while CRH neurons were found to be glutamatergic in the rat paraventricular nucleus of the hypothalamus (PVN) (Dabrowska et al., 2013). In the current study, CRH+ BNST cells were found to contain both glutamatergic and GABAergic subpopulations (Figure 11). Furthermore, the composition of CRH+ cells varies with subregions, as almost all the CRH neurons were found to be GABAergic in the dorsal lateral BNST ( $98.2 \pm 1$  %), and in comparison,  $78.6 \pm 2.8$  % and  $69.7 \pm 4.0$  % of CRH neurons are GABAergic in the dorsal medial and ventral BNST, respectively (Table 3).

Only a small amount of ChAT+ labeling was found in the BNST of ChAT-Cre; Ai9 mice (data not shown) as compared to basal forebrain regions (such as the medial septum and

diagonal band of Broca) which contained a large number of cholinergic neurons. The few ChAT+ neurons found in the adBNST were localized near the jcBNST, and quantitative analysis confirmed that only 0.5% of the total neurons were ChAT+ ( $0.84 \pm 0.10$  cells/mm<sup>2</sup>). A similar pattern was found in the vBNST as about 1.5% of the neurons were ChAT+ ( $2.03 \pm 0.55$  cells/mm<sup>2</sup>) near lateral vBNST. In general, cholinergic neurons were not found to be critically associated with the BNST, which validates evidence found in previous studies (Bota et al., 2012).

## DISCUSSION

Identification and characterization of specific subsets of BNST neurons are necessary and fundamental steps in order to understand specific BNST functional involvement. The goal of the current study is to identify and characterize specific BNST cell types aided by genetic cell targeting in the mouse. Using this approach, we established the presence and distribution of excitatory glutamatergic neurons in both adBNST and vBNST. Excitatory neurons were shown to be a major subpopulation of BNST cells in both dorsal and ventral BNST regions. These are the same areas that contain relatively high percentages of BNST neurons expressing CaMKII $\alpha$  and EAAC+/GAD- (markers of excitatory cells). This major finding has impact on our understanding of the BNST cell types. Previously, the lack of excitatory neurons reported in rodent dorsal BNST was partial because it was based on the use of VGLUT markers, particularly VGLUT2 (Poulin et al., 2009). The present study confirmed the presence of VGLUT2+ cells is sparse and mostly located in the vBNST. Nevertheless, inhibitory GABAergic neurons make up a predominant portion of the general makeup of adBNST, which is contrary to the makeup of excitatory and inhibitory neurons in the cerebral cortex in general.

### Methodological Considerations

As demonstrated above, our control immunochemical staining and *in situ* gene expression data of Allen Mouse Brain Atlas (Available from: <http://mouse.brain-map.org/>) generally supports the correspondence of Cre/transgenic expression to specific chemical markers in the BNST. In addition, previous studies have confirmed Cre eutopic expression in the brain regions of GAD2-Cre, CRH-Cre, Camk2a-Cre, VGLUT2-Cre, and PV-Cre, SOM-Cre and VIP-Cre. According to Taniguchi et al. (2011), in adult brain regions of the GAD2-Cre mouse crossed to a reporter line (GAD2-Cre; RCE-LoxP), Cre-activated RCE reporter GFP expression is “almost entirely restricted to GABAergic neurons and includes almost all GABAergic neurons”. Specifically, they reported that in the primary somatosensory cortex, the percentage of GFP neurons that were GAD67 immunopositive was  $92\% \pm 2.1\%$  and the fraction of GAD67+ cells expressing GFP was  $91\% \pm 2.9\%$ . For the GAD-GFP mouse used in the present study, it has been extensively characterized. It was reported that the distribution pattern of GFP-positive somata was the same as that of the GAD67 *in situ* hybridization signal in the adult central nervous system, and that there was no apparent ectopic GFP expression in GAD67-negative cells nor any apparent lack of GFP expression in GAD67-positive neurons (Tamamaki et al., 2003). In mouse visual cortex, our unpublished double immunostaining observations independently verified the fidelity of using PV-Cre, SOM-Cre and VIP-Cre for surrogates of PV+, SOM+ and VIP+ neurons. By

crossing VGLUT2-Cre mice with lox-GFP reporter mice, Vong et al. (2011) confirmed that Cre is ectopically expressed by comparing GFP expression and *in situ* hybridization patterns. Supporting the use of CRH-Cre;Ai9 mice in characterizing BNST neurons, Chen et al. (2015) reported that in the PVN region of CRH-Cre; Ai14 tdTomato mice, CRH-immunoreactivity was observed in  $93.3 \pm 1.2\%$  of the tdTomato neurons, and  $95.1 \pm 1.2\%$  CRH-expressing somata coexpressed tdTomato. They also noted the colocalization of tdTomato and CRH peptide expression in the BNST.

As Camk2a and PV genes turn on around the mouse age of postnatal two weeks, their permanent reporter allele activation through Cre/loxP recombination is restricted to the mouse brains beyond the two week old age. However, this is not the case for calretinin (CR), given that CR is known to transiently express in the neocortex and hippocampus during early development. Although CR is considered as an inhibitory neuronal mark, it is recently reported that in the mature visual cortex of the CR-Cre mouse line, only a minority of the cells that have expressed calretinin and Cre-recombinase during their lifetime is GABAergic and only about 20% are immunoreactive for calretinin (Camillo et al., 2014). In our previous study (San Antonio et al., 2014), we found that in the CR-Cre; Ai9 mouse, dentate granule cells express strong red fluorescent (tdTomato) proteins so that their axon bundles are fluorescently visible in hippocampal sections. These concerns are further supported by our present finding that CR-Cre; Ai9 did not have robust localization of CR immunoreactivity. The caveat of transient Cre activity in early development can be overcome by using CR-CreER mice in which Cre gene activity is inducible by tamoxifen administration.

Although genetic targeting has advantages of consistency and repeatability, there are potential serious technical limitations. A major caveat includes whether specific transgenic mice yield labeling profiles that are inclusive of the entire population, or just provide fractions of representative samples. In the present study, we found that genetic labels in both GAD67-GFP and GAD2-Cre; Ai9 mice showed good fidelity in adBNST, as 98% of genetic labeled cells were shown to be positive for GABA immunostaining and 90% of GABA immunopositive cells showed genetic labels. However, while GAD-GFP transgenic labels performed better, only 43% of GABA immunopositive cells were detected for tdTomato expression in the vBNST of the GAD2-Cre; Ai9 mouse. Thus if GAD2-Cre mice are used for labeling GABAergic cells in vBNST, this concerns an underrepresentation of GABA+ cells in the Cre mouse line. Similarly, this concern applies to intending to use Camk2a-Cre; Ai9 mice to label CaMKII immunopositive cells in the vBNST. With this in mind, we have adopted the merits of different methods including immunostaining and *in situ*-based approaches, and first establish the appropriateness of using transgenic mice for the present study.

### Specific BNST neuronal types and distinct subregions

Overall, our data reveals that adBNST and vBNST have differential compositions of GABAergic and glutamatergic neuronal types. Generally, the dorsal portion of the BNST was found to have a higher neuronal density than the vBNST. They differed in relative proportions of excitatory versus inhibitory neurons. The adBNST was found to have a great majority of GABAergic inhibitory neurons (~69%) and only 14% of glutamatergic

excitatory neurons. In comparison, the vBNST contains relatively equal proportions of GABAergic inhibitory neurons (33%) and excitatory glutamatergic neurons (31%). These findings provide neuronal makeup differences corroborating the known functional differences of adBNST and vBNST (Dong et al., 2000; Dong and Swanson, 2004; Jennings et al., 2013; Kim et al., 2013; Poulin et al., 2009). The lateral and medial portions of adBNST (ovBNST and alBNST, versus ambBNST) were found to be distinguishable in terms of marker expression of CaMKII $\alpha$ , SOM and VIP. The ambBNST tended to have less dense GAD+ cells and CRH+ cells than the rest of adBNST. The differences seen in the adBNST and vBNST cell makeup and marker expression may underlie functional differences of specific adBNST subregions for stress modulation versus central autonomic control, respectively (Crestani et al., 2013; Dong and Swanson, 2006; Walker et al., 2003).

The ovBNST subregion contains significant numbers of CaMKII $\alpha$ + cells and SOM+ cells, along with very distinct VIP+ axonal plexuses found only within the ovBNST. The findings of earlier anatomical studies indicate that the midbrain raphe nuclei, the periaqueductal gray and the amygdala are the origins of the VIP+ fiber plexus found (Eiden et al., 1985; Petit et al., 1995). In addition, the BNST was found to be influenced by the circadian rhythm control from the suprachiasmatic nucleus (SCN) (Amir et al., 2004). It is possible that the VIP+ fibers may ascend from the SCN, which is known to have concentrated VIP+ neurons. However, the potential direct connections between the SCN and ovBNST have not been established. The Xu lab is currently working on mapping the input sources and characterizing the nature of VIP+ fiber plexus using newly developed viral tracing tools. Likewise, the jcBNST (another subregion in the adBNST) was found to contain both concentrated CaMKII $\alpha$ + and GAD+ cells with VIP+ axonal plexuses running through the more anterior region of the jcBNST, and ChAT+ cells were found mainly near the lining of the internal capsule and surrounding the jcBNST region. Thus, unique spatial distributions of molecular and neurochemical expression found in the current study can facilitate BNST subregional delineation; the expression of CaMKII $\alpha$ +, GAD2 and VIP may be effectively used to localize the ovBNST and jcBNST.

Because CRH+ neurons are almost exclusively located in the BNST but not the surrounding regions, CRH can be used as a specific targeting marker for the BNST. The CRH-Cre mouse may be a useful tool in additional physiological and functional studies. Furthermore, the distribution of CRH neurons appears to vary markedly between rat and mouse. In the rat, CRH is densely expressed in neurons within oval and fusiform nuclei, with some representation of cells in the dorsomedial nucleus. On the contrary, mouse CRH neurons appear to be widely scattered throughout both dorsal and ventral subdivisions in BNST. This species difference of CRH+ neuronal distribution suggests that the mouse may not show the same degree of well-organized BNST subdivision as in the rat, and further suggests that functional roles of these BNST subregions may be potentially different across the two species.

Since considerable progress has been made in correlating cell types with chemical markers, particularly in the neocortex and hippocampus, it is suspected that some of neurochemical markers examined in the current study can be closely correlated with morphology and/or physiology of specific BNST neuron types. This is supported by the fact that lack of PV+

expression in BNST neurons is correlated to the apparent absence of a fast-spiking electrophysiology phenotype reported in the BNST literature (Egli and Winder, 2003; Hammack et al., 2007; Rodriguez-Sierra et al., 2013). By using the same genetic approach employed in the present study, we can visualize morphology and characterize physiology of Cre-defined BNST cell types to establish neurochemical and cell-type specific physiology correlations. Furthermore, by using the new information derived from the present study, specific cell types can be targeted to map their circuit connections and assess their functional roles in BNST-associated behaviors.

Together, the present study has uncovered new information on specific inhibitory and excitatory neurons in the BNST, which provides an important basis for cell-type specific circuit and functional studies of the BNST.

## Acknowledgments

This work was partially funded by US National Institutes of Health grants NS078434, MH105427 and a NARSAD Young Investigator Award to X.X. This work was also made possible, in part, through access to the confocal facility of the Optical Biology Shared Resource of the Cancer Center Support Grant (CA-62203) at the University of California, Irvine.

## References

- Amir S, Lamont EW, Robinson B, Stewart J. A circadian rhythm in the expression of PERIOD2 protein reveals a novel SCN-controlled oscillator in the oval nucleus of the bed nucleus of the stria terminalis. *The Journal of neuroscience: the official journal of the Society for Neuroscience*. 2004; 24:781–790. [PubMed: 14749422]
- Bota M, Sporns O, Swanson LW. Neuroinformatics analysis of molecular expression patterns and neuron populations in gray matter regions: the rat BST as a rich exemplar. *Brain Res*. 2012; 1450:174–193. [PubMed: 22421015]
- Camillo D, Levelt CN, Heimel JA. Lack of functional specialization of neurons in the mouse primary visual cortex that have expressed calretinin. *Front Neuroanat*. 2014; 8:89. [PubMed: 25237298]
- Chen Y, Bender RA, Frotscher M, Baram TZ. Novel and transient populations of corticotropin-releasing hormone-expressing neurons in developing hippocampus suggest unique functional roles: a quantitative spatiotemporal analysis. *The Journal of neuroscience: the official journal of the Society for Neuroscience*. 2001; 21:7171–7181. [PubMed: 11549728]
- Chen Y, Molet J, Gunn BG, Ressler K, Baram TZ. Diversity of Reporter Expression Patterns in Transgenic Mouse Lines Targeting Corticotropin-Releasing Hormone-Expressing Neurons. *Endocrinology*. 2015; 156:4769–4780. [PubMed: 26402844]
- Conti F, DeBiasi S, Minelli A, Rothstein JD, Melone M. EAAC1, a high-affinity glutamate transporter, is localized to astrocytes and gabaergic neurons besides pyramidal cells in the rat cerebral cortex. *Cereb Cortex*. 1998; 8:108–116. [PubMed: 9542890]
- Crestani CC, Alves FH, Gomes FV, Resstel LB, Correa FM, Herman JP. Mechanisms in the bed nucleus of the stria terminalis involved in control of autonomic and neuroendocrine functions: a review. *Current neuropharmacology*. 2013; 11:141–159. [PubMed: 23997750]
- Dabrowska J, Hazra R, Guo JD, Dewitt S, Rainnie DG. Central CRF neurons are not created equal: phenotypic differences in CRF-containing neurons of the rat paraventricular hypothalamus and the bed nucleus of the stria terminalis. *Front Neurosci*. 2013; 7:156. [PubMed: 24009552]
- Deisseroth K. Circuit dynamics of adaptive and maladaptive behaviour. *Nature*. 2014; 505:309–317. [PubMed: 24429629]
- Dong H, Petrovich GD, Swanson LW. Organization of projections from the juxtacapsular nucleus of the BST: a PHAL study in the rat. *Brain research*. 2000; 859:1–14. [PubMed: 10720609]

- Dong HW, Petrovich GD, Swanson LW. Topography of projections from amygdala to bed nuclei of the stria terminalis. *Brain research Brain research reviews*. 2001; 38:192–246. [PubMed: 11750933]
- Dong HW, Swanson LW. Organization of axonal projections from the anterolateral area of the bed nuclei of the stria terminalis. *J Comp Neurol*. 2004; 468:277–298. [PubMed: 14648685]
- Dong HW, Swanson LW. Projections from bed nuclei of the stria terminalis, dorsomedial nucleus: implications for cerebral hemisphere integration of neuroendocrine, autonomic, and drinking responses. *J Comp Neurol*. 2006; 494:75–107. [PubMed: 16304681]
- Egli RE, Winder DG. Dorsal and ventral distribution of excitable and synaptic properties of neurons of the bed nucleus of the stria terminalis. *Journal of neurophysiology*. 2003; 90:405–414. [PubMed: 12649311]
- Eiden LE, Hokfelt T, Brownstein MJ, Palkovits M. Vasoactive intestinal polypeptide afferents to the bed nucleus of the stria terminalis in the rat: an immunohistochemical and biochemical study. *Neuroscience*. 1985; 15:999–1013. [PubMed: 3900807]
- Georges F, Aston-Jones G. Potent regulation of midbrain dopamine neurons by the bed nucleus of the stria terminalis. *J Neurosci*. 2001; 21:RC160. [PubMed: 11473131]
- Guillery RW. On counting and counting errors. *J Comp Neurol*. 2002; 447:1–7. [PubMed: 11967890]
- Hammack SE, Mania I, Rainnie DG. Differential expression of intrinsic membrane currents in defined cell types of the anterolateral bed nucleus of the stria terminalis. *Journal of neurophysiology*. 2007; 98:638–656. [PubMed: 17537902]
- Hazra R, Guo JD, Ryan SJ, Jasnow AM, Dabrowska J, Rainnie DG. A transcriptomic analysis of type I–III neurons in the bed nucleus of the stria terminalis. *Mol Cell Neurosci*. 2011; 46:699–709. [PubMed: 21310239]
- Jennings JH, Sparta DR, Stamatakis AM, Ung RL, Pleil KE, Kash TL, Stuber GD. Distinct extended amygdala circuits for divergent motivational states. *Nature*. 2013; 496:224–228. [PubMed: 23515155]
- Johansen JP. Neuroscience: anxiety is the sum of its parts. *Nature*. 2013; 496:174–175. [PubMed: 23515160]
- Ju G, Swanson LW. Studies on the cellular architecture of the bed nuclei of the stria terminalis in the rat: I. Cytoarchitecture. *The Journal of comparative neurology*. 1989; 280:587–602. [PubMed: 2708568]
- Ju G, Swanson LW, Simerly RB. Studies on the cellular architecture of the bed nuclei of the stria terminalis in the rat: II. Chemoarchitecture. *The Journal of comparative neurology*. 1989; 280:603–621. [PubMed: 2468695]
- Kim SY, Adhikari A, Lee SY, Marshel JH, Kim CK, Mallory CS, Lo M, Pak S, Mattis J, Lim BK, et al. Diverging neural pathways assemble a behavioural state from separable features in anxiety. *Nature*. 2013; 496:219–223. [PubMed: 23515158]
- Larriva-Sahd J. Juxtacapsular nucleus of the stria terminalis of the adult rat: extrinsic inputs, cell types, and neuronal modules: a combined Golgi and electron microscopic study. *The Journal of comparative neurology*. 2004; 475:220–237. [PubMed: 15211463]
- Larriva-Sahd J. Histological and cytological study of the bed nuclei of the stria terminalis in adult rat. II. Oval nucleus: extrinsic inputs, cell types, neuropil, and neuronal modules. *J Comp Neurol*. 2006; 497:772–807. [PubMed: 16786552]
- Lein ES, Hawrylycz MJ, Ao N, Ayres M, Bensinger A, Bernard A, Boe AF, Boguski MS, Brockway KS, Byrnes EJ, et al. Genome-wide atlas of gene expression in the adult mouse brain. *Nature*. 2007; 445:168–176. [PubMed: 17151600]
- Madisen L, Zwingman TA, Sunkin SM, Oh SW, Zariwala HA, Gu H, Ng LL, Palmiter RD, Hawrylycz MJ, Jones AR, et al. A robust and high-throughput Cre reporting and characterization system for the whole mouse brain. *Nat Neurosci*. 2010; 13:133–140. [PubMed: 20023653]
- Magableh A, Lundy R. Somatostatin and corticotrophin releasing hormone cell types are a major source of descending input from the forebrain to the parabrachial nucleus in mice. *Chemical senses*. 2014; 39:673–682. [PubMed: 25086873]
- McDonald AJ. Neurons of the bed nucleus of the stria terminalis: a golgi study in the rat. *Brain research bulletin*. 1983; 10:111–120. [PubMed: 6824959]

- Moga MM, Saper CB, Gray TS. Bed nucleus of the stria terminalis: cytoarchitecture, immunohistochemistry, and projection to the parabrachial nucleus in the rat. *J Comp Neurol*. 1989; 283:315–332. [PubMed: 2568370]
- Petit JM, Luppi PH, Peyron C, Rampon C, Jouvet M. VIP-like immunoreactive projections from the dorsal raphe and caudal linear raphe nuclei to the bed nucleus of the stria terminalis demonstrated by a double immunohistochemical method in the rat. *Neurosci Lett*. 1995; 193:77–80. [PubMed: 7478163]
- Poulin JF, Arbour D, Laforest S, Drolet G. Neuroanatomical characterization of endogenous opioids in the bed nucleus of the stria terminalis. *Progress in neuro-psychopharmacology & biological psychiatry*. 2009; 33:1356–1365. [PubMed: 19583989]
- Rodriguez-Sierra OE, Turesson HK, Pare D. Contrasting distribution of physiological cell types in different regions of the bed nucleus of the stria terminalis. *J Neurophysiol*. 2013; 110:2037–2049. [PubMed: 23926040]
- San Antonio A, Liban K, Ikrar T, Tsyganovskiy E, Xu X. Distinct physiological and developmental properties of hippocampal CA2 subfield revealed by using anti-Purkinje cell protein 4 (PCP4) immunostaining. *J Comp Neurol*. 2014; 522:1333–1354. [PubMed: 24166578]
- Sawchenko PE. Adrenalectomy-induced enhancement of CRF and vasopressin immunoreactivity in parvocellular neurosecretory neurons: anatomic, peptide, and steroid specificity. *J Neurosci*. 1987; 7:1093–1106. [PubMed: 3553442]
- Silberman Y, Matthews RT, Winder DG. A corticotropin releasing factor pathway for ethanol regulation of the ventral tegmental area in the bed nucleus of the stria terminalis. *J Neurosci*. 2013; 33:950–960. [PubMed: 23325234]
- Silberman Y, Winder DG. Emerging role for corticotropin releasing factor signaling in the bed nucleus of the stria terminalis at the intersection of stress and reward. *Frontiers in psychiatry*. 2013; 4:42. [PubMed: 23755023]
- Sun Y, Nguyen AQ, Nguyen JP, Le L, Saur D, Choi J, Callaway EM, Xu X. Cell-type-specific circuit connectivity of hippocampal CA1 revealed through Cre-dependent rabies tracing. *Cell Rep*. 2014; 7:269–280. [PubMed: 24656815]
- Swanson LW, Sawchenko PE, Rivier J, Vale WW. Organization of ovine corticotropin-releasing factor immunoreactive cells and fibers in the rat brain: an immunohistochemical study. *Neuroendocrinology*. 1983; 36:165–186. [PubMed: 6601247]
- Tamamaki N, Yanagawa Y, Tomioka R, Miyazaki J, Obata K, Kaneko T. Green fluorescent protein expression and colocalization with calretinin, parvalbumin, and somatostatin in the GAD67-GFP knock-in mouse. *J Comp Neurol*. 2003; 467:60–79. [PubMed: 14574680]
- Taniguchi H, He M, Wu P, Kim S, Paik R, Sugino K, Kvitsiani D, Fu Y, Lu J, Lin Y, et al. A resource of Cre driver lines for genetic targeting of GABAergic neurons in cerebral cortex. *Neuron*. 2011; 71:995–1013. [PubMed: 21943598]
- Turesson HK, Rodriguez-Sierra OE, Pare D. Intrinsic connections in the anterior part of the bed nucleus of the stria terminalis. *J Neurophysiol*. 2013; 109:2438–2450. [PubMed: 23446692]
- Vong L, Ye C, Yang Z, Choi B, Chua S Jr, Lowell BB. Leptin action on GABAergic neurons prevents obesity and reduces inhibitory tone to POMC neurons. *Neuron*. 2011; 71:142–154. [PubMed: 21745644]
- Walker DL, Toufexis DJ, Davis M. Role of the bed nucleus of the stria terminalis versus the amygdala in fear, stress, and anxiety. *European journal of pharmacology*. 2003; 463:199–216. [PubMed: 12600711]
- Wood RI, Swann JM. The bed nucleus of the stria terminalis in the Syrian hamster: subnuclei and connections of the posterior division. *Neuroscience*. 2005; 135:155–179. [PubMed: 16084647]
- Xu X, Roby KD, Callaway EM. Mouse cortical inhibitory neuron type that coexpresses somatostatin and calretinin. *The Journal of comparative neurology*. 2006; 499:144–160. [PubMed: 16958092]
- Xu X, Roby KD, Callaway EM. Immunochemical characterization of inhibitory mouse cortical neurons: three chemically distinct classes of inhibitory cells. *The Journal of comparative neurology*. 2010; 518:389–404. [PubMed: 19950390]
- Yan XX, Toth Z, Schultz L, Ribak CE, Baram TZ. Corticotropin-releasing hormone (CRH)-containing neurons in the immature rat hippocampal formation: light and electron microscopic features and

colocalization with glutamate decarboxylase and parvalbumin. *Hippocampus*. 1998; 8:231–243.  
[PubMed: 9662138]

Author Manuscript

Author Manuscript

Author Manuscript

Author Manuscript

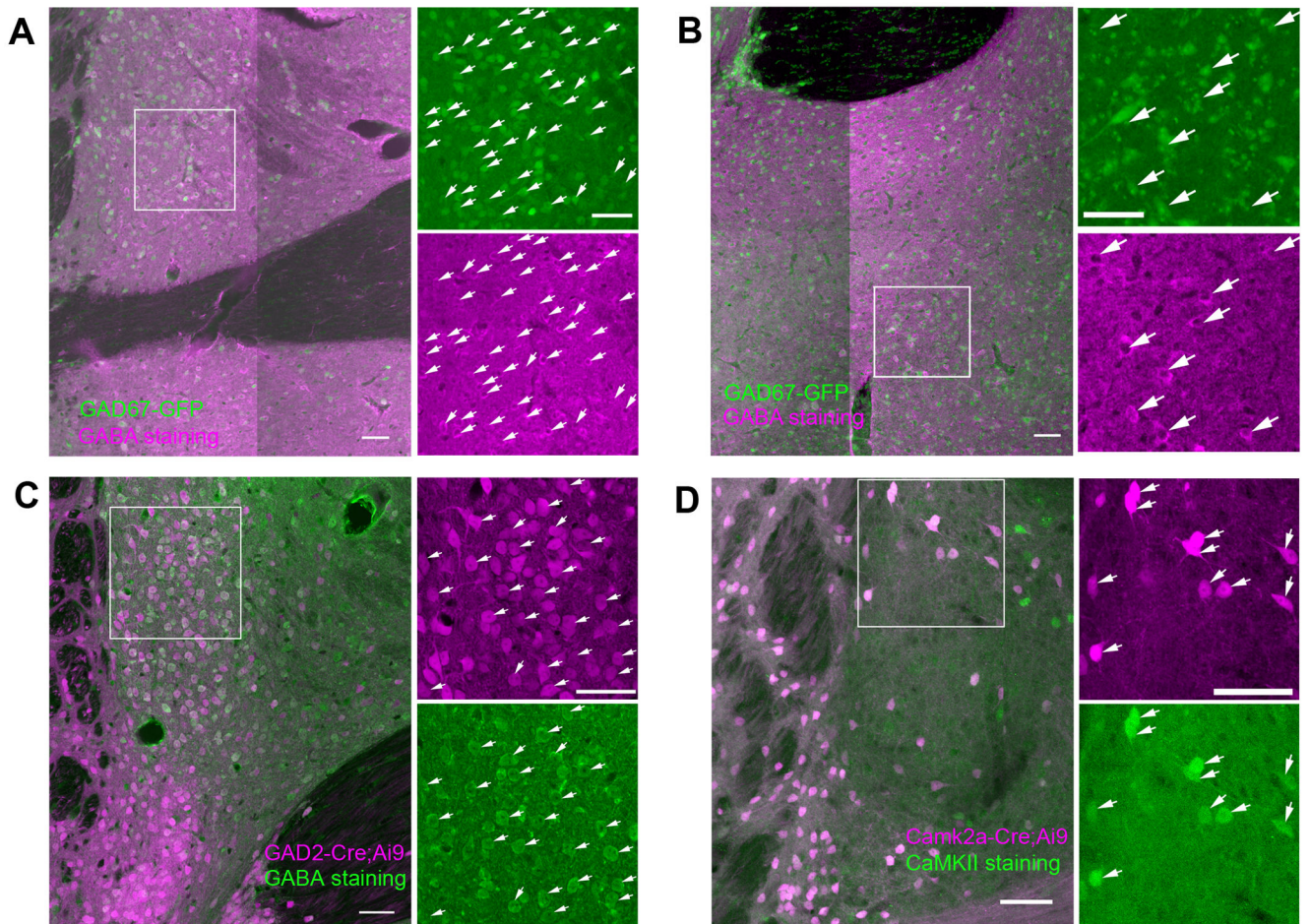


**Figure 1. Cre/transgenic expression corresponds to chemical marker expression in the mouse BNST**

(A). GAD67-GFP expression (green) in the GAD67-GFP mouse labels almost all GABA positive neurons confirmed by GABA immunostaining (red) in the dorsal BNST. (Left). A representative image with red and green channels merged. (Right). Enlarged panels from the white square region in the left with GAD67-GFP labeling at the top and GABA immunostaining at the bottom. The white arrows indicate selected examples of co-localization. (B–D) are similarly formatted as A. (B). GAD67-GFP labels in the ventral BNST of the GAD67-GFP mouse also have good co-localization with GABA immunoreactivity. (C). GAD2-Cre expression (tdTomato expression, red) in the GAD2-Cre; Ai9 mouse corresponds to GABA immunoreactivity positive neurons confirmed by GABA immunostaining (green). (D). Camk2a-Cre expression (tdTomato expression, red) in the Camk2a-Cre; Ai9 mouse is positive for CaMKII immunostaining (green). Scale bar: 50  $\mu$ m.

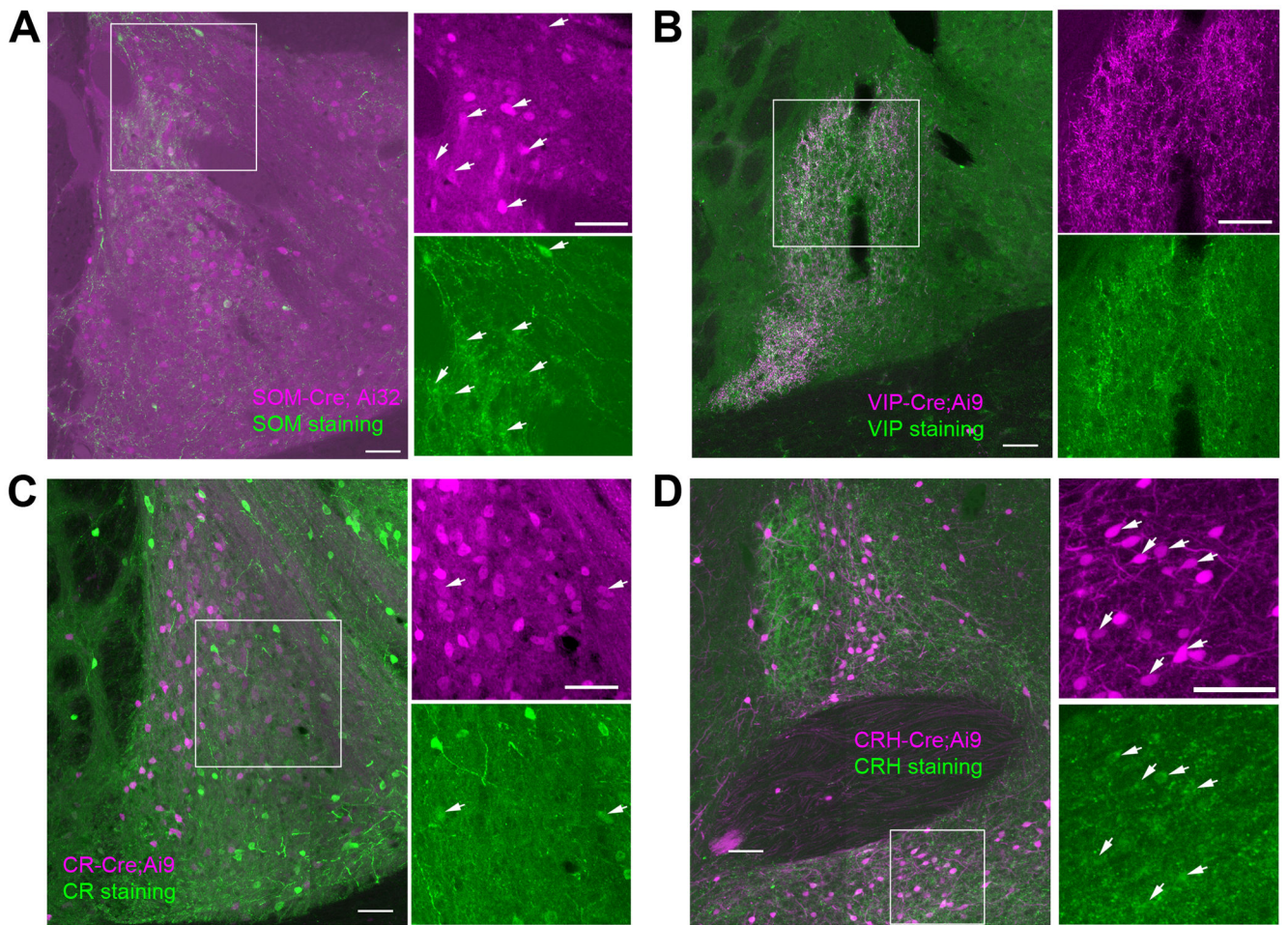


**Figure 2. SOM-Cre, VIP-Cre, CR-Cre and CRH-Cre expression shows variable correspondence to immunochemical staining**

(A). SOM-Cre expression (YFP expression, red pseudocolor) in the SOM-Cre; Ai32 mouse have some correspondence to SOM immunoreactivity (green). (B). VIP-Cre expression (tdTomato expression, red) in the VIP-Cre; Ai9 mouse is verified by VIP immunoreactivity (green). (C). CR-Cre expression (tdTomato expression, red) in the CR-Cre; Ai9 mouse shows low colocalization with CR immunoreactivity (green). (D). CRH-Cre expression (tdTomato expression, red) in the CRH-Cre; Ai9 mouse has correspondence to CRH immunoreactivity (green). Scale bar: 50  $\mu$ m.

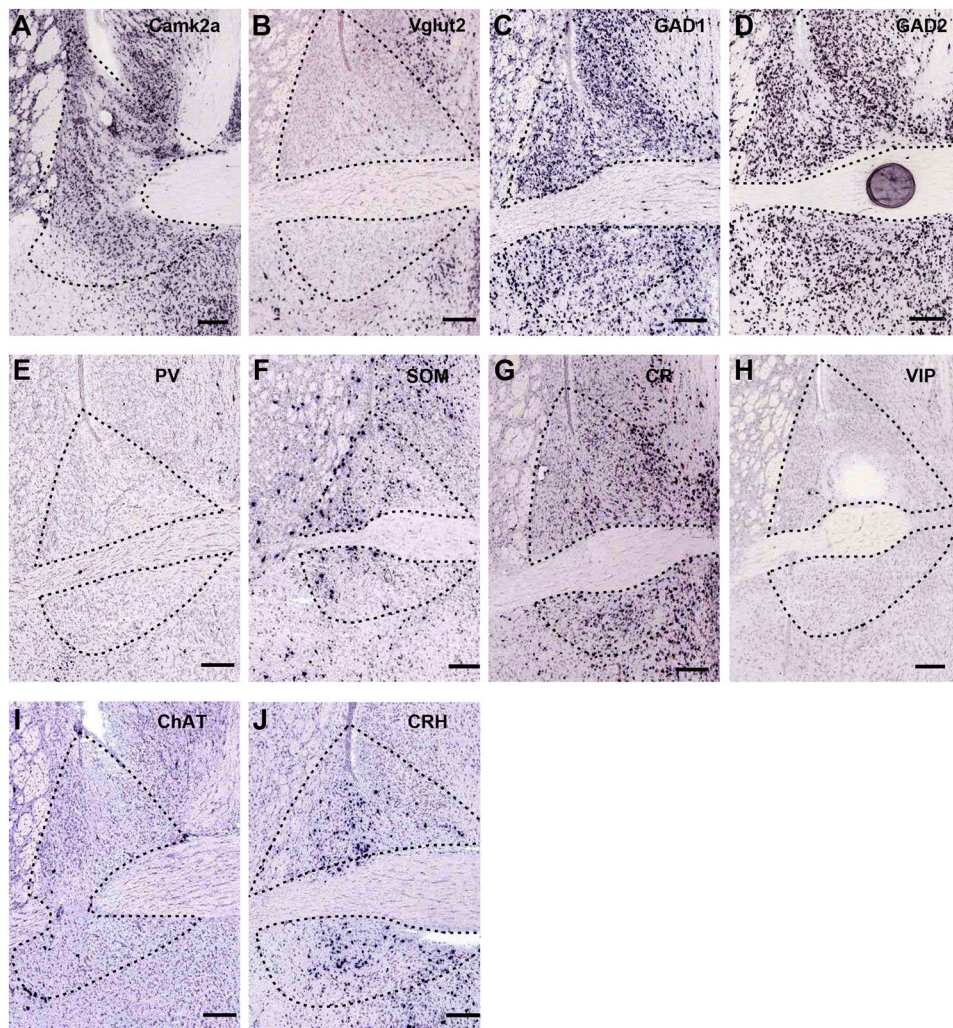


**Figure 3. Example images of *in situ* specific mRNA distribution in the BNST**  
 The *in situ* hybridization image data of A–K correspond to the markers of Camk2a, VGLUT2, GAD1, GAD2, PV, SOM, CR, VIP, ChAT and CRH. Scale bar: 200  $\mu$ m. These Allen Mouse Brain Atlas images are obtained and modified from the Allen Institute for Brain Science website: [http://mouse.brain-map.org/experiment/thumbnails/100048576?image\\_type=atlas](http://mouse.brain-map.org/experiment/thumbnails/100048576?image_type=atlas) (Image credit: Allen Institute for Brain Science) (Lein et al., 2007).

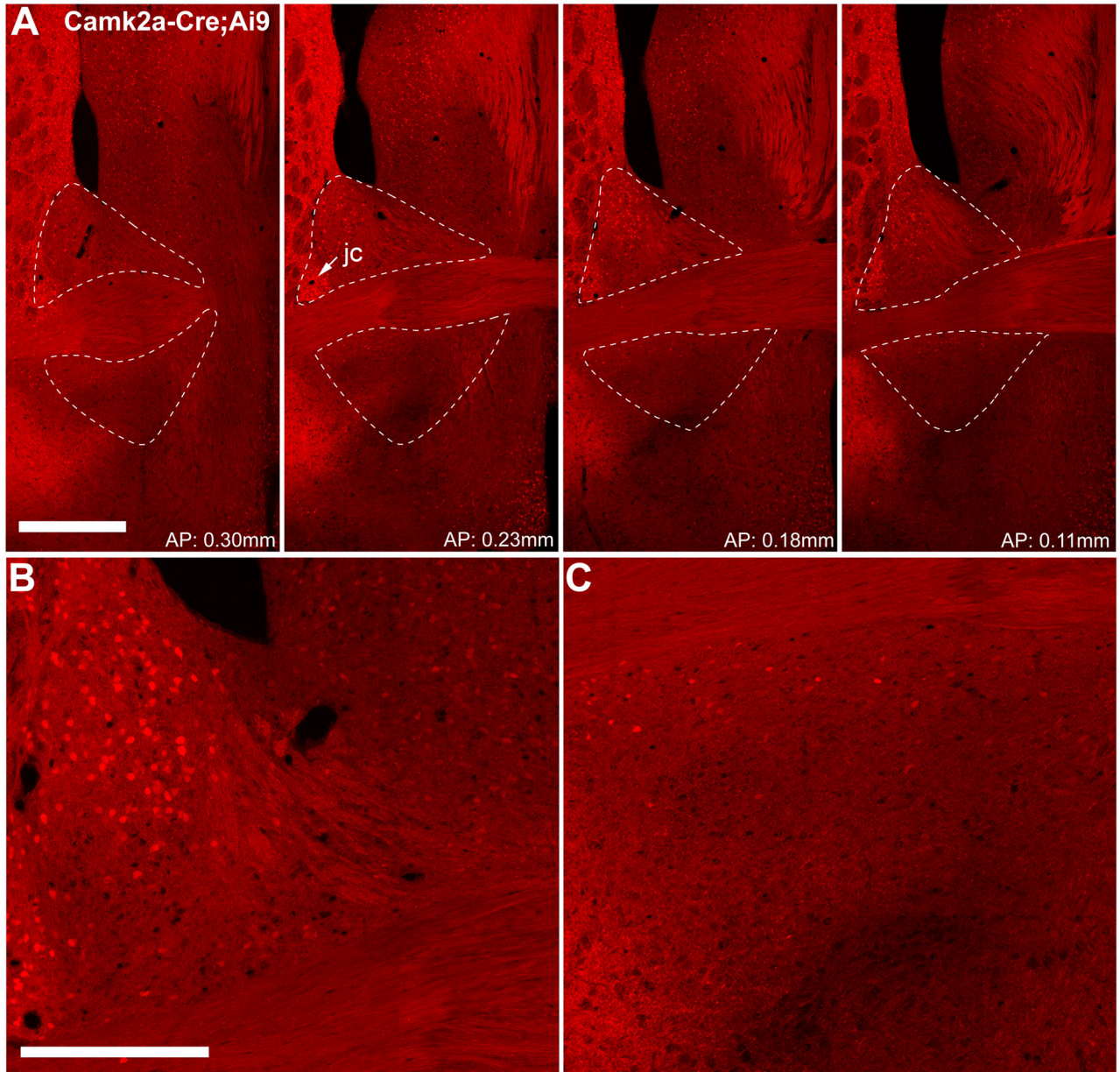


**Figure 4. Assessment of the distribution of CaMKII $\alpha$ -expressing neurons in the bed nucleus of the stria terminalis (BNST) using the Camk2a-Cre; Ai9 mouse**

(A) CaMKII $\alpha$ + neurons expressing the red fluorescent protein (tdTomato) are distributed mainly in the adBNST, while fewer cells in the vBNST at various levels from anterior-posterior (AP) 0.30 mm to 0.11 mm. (B) Enlarged image of the adBNST at AP 0.18mm. Most CaMKII $\alpha$ + neurons are localized at the lateral portions of the adBNST, near the lining of the internal capsule and the oval BNST (ovBNST). Relatively sparse CaMKII $\alpha$ + cells are found in ambBNST. (C) Enlarged image of vBNST at AP 0.18 mm. Scale Bar: 250 $\mu$ m (A), 100 $\mu$ m (B, C). The BNST contour (dashed lines) is drawn in consideration that the BNST is enclosed by the lateral ventricle, lateral septum, caudate putamen, anterior commissure, and ventral pallidum, the hypothalamic preoptic area, and based on gross cytoarchitecture

features seen in DAPI staining, as well as the patterns of GAD65/67 expression (Figure 6) and CRH (Figure 10) expression. The same conventions apply to the following figures.

Author Manuscript

Author Manuscript

Author Manuscript

Author Manuscript

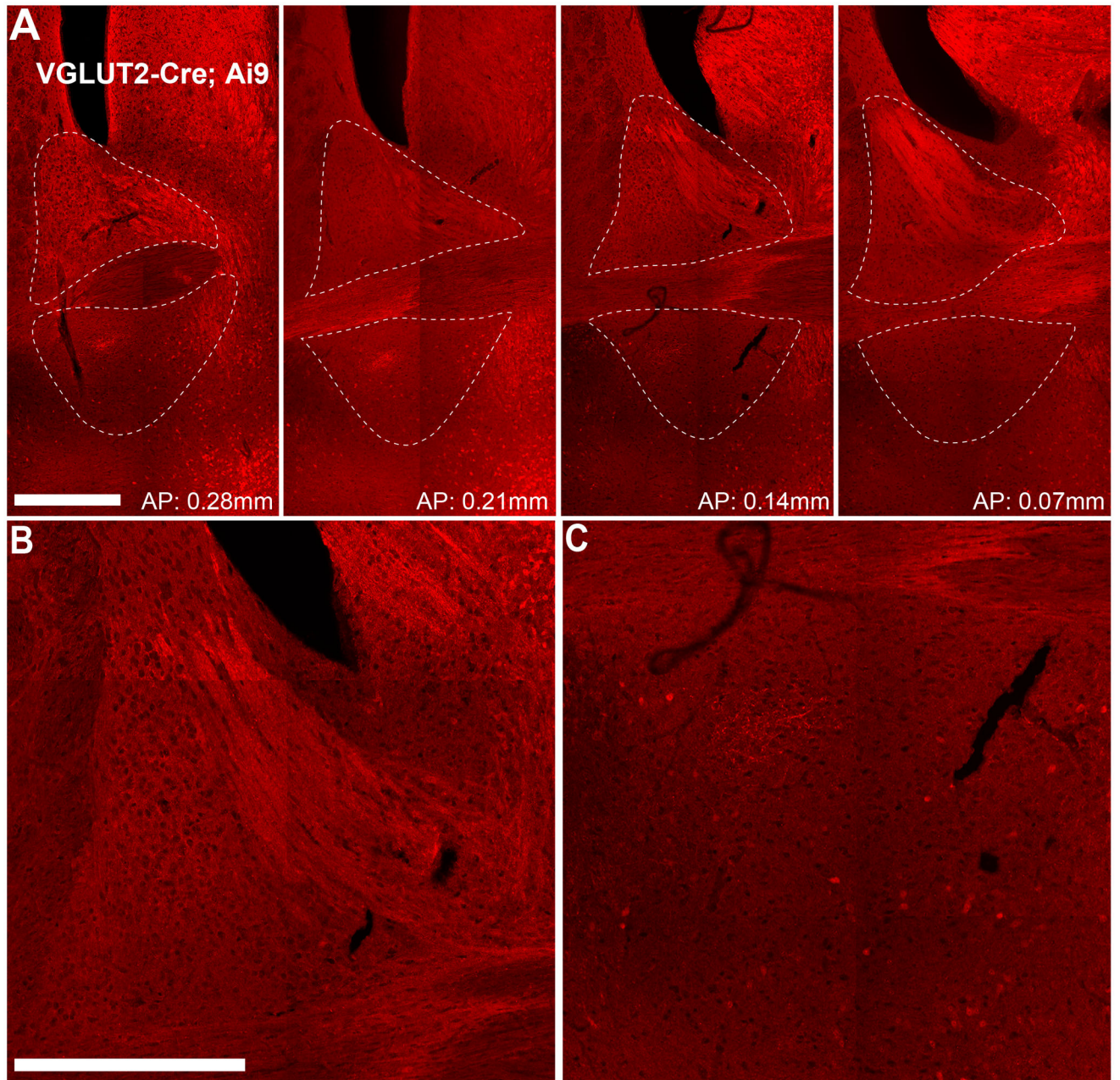


**Figure 5. Assessment of the distribution of VGLUT2+ neurons in the BNST using the VGLUT2-Cre; Ai9 mouse**  
 (A) VGLUT2+ neurons are essentially absent in adBNST and sparse in vBNST (B) Enlarged image of the adBNST at AP 0.14 mm. (C) Enlarged image of the vBNST at AP 0.14 mm. Scale Bar: 250 $\mu$ m (A), 100 $\mu$ m (B, C).

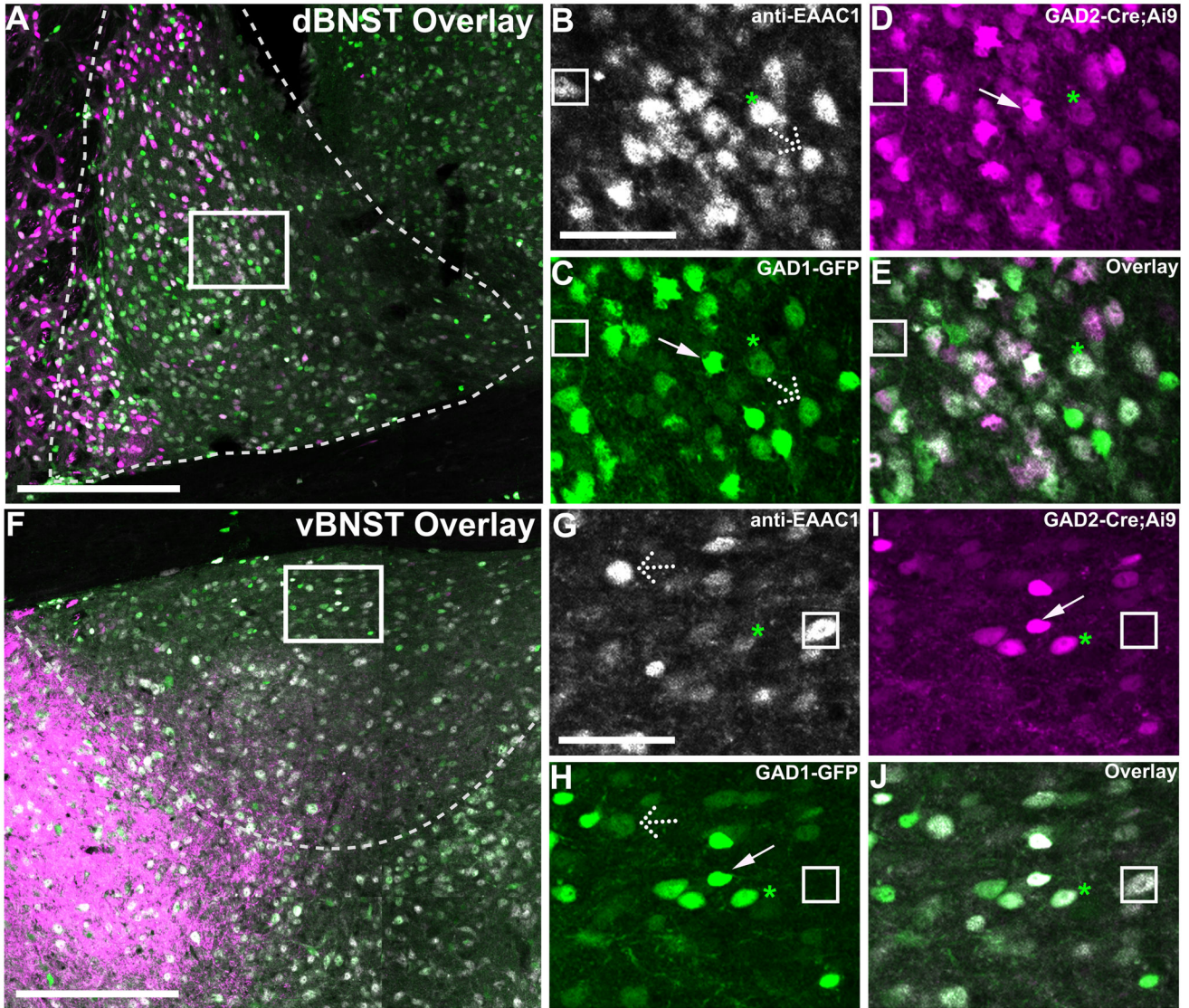


**Figure 6. Evaluation of excitatory glutamatergic neuronal distribution in the BNST with immunostaining against excitatory amino acid transporter type1 (EAAC1) in sections of cross-bred mice of GAD2-Cre; Ai9/GAD67-GFP. Colocalization is examined across EAAC1+, GAD67+, and GAD65+ cells**

(A) An example image showing a triple labeled adBNST section. EAAC1 staining is shown in white, GAD1 (GAD67) expressing neurons are labeled with GFP, while GAD2 (GAD65) expressing neurons are labeled with the red fluorescent protein (tdTomato). (F) An example image showing a triple labeled vBNST section. (B–E) and (G–J), enlarged view of the white box in A and F, respectively. EAAC1 staining is shown in white, GAD67 (GAD1) expression is shown in green, and GAD65 (GAD2) expression is shown in red. Labels are merged in the overlay, respectively. Dotted arrows indicate colocalization of GAD67 and EAAC1 in an example neuron. Yellow arrows indicate colocalization of GAD67 and GAD65 in an example neuron, while asterisks point at triple colocalization of GAD67, GAD65, and EAAC. The EAAC1+ neurons that are not colocalized with GAD (white

squares in B–E and G–J) are considered excitatory glutamatergic neurons in the BNST.  
Scale bars: 250 $\mu$ m in (A, F), 50 $\mu$ m in (B and G).

Author Manuscript

Author Manuscript

Author Manuscript

Author Manuscript

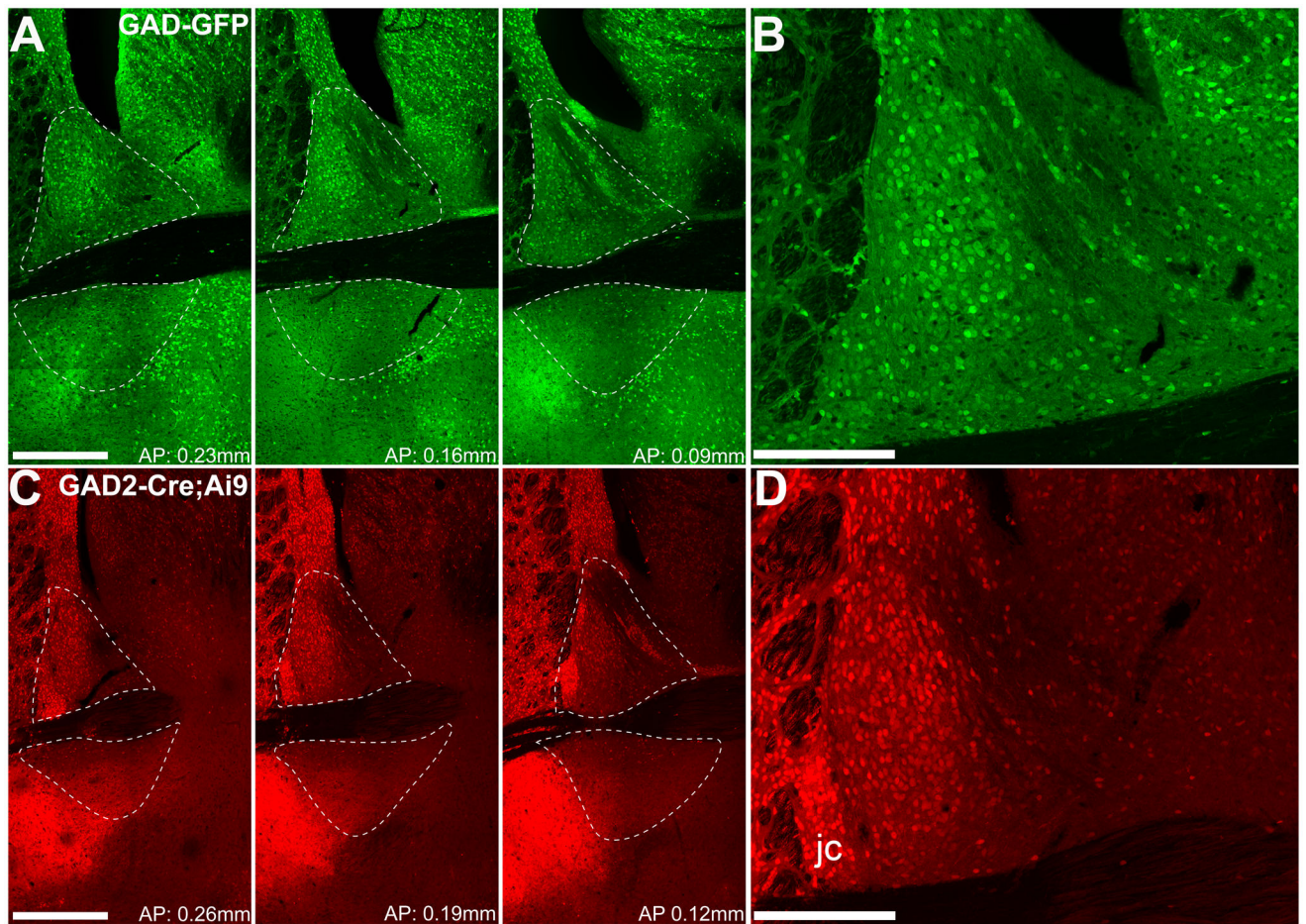


**Figure 7. Assessment of the distribution of inhibitory GABAergic neurons in the BNST using the mice of GAD1-GFP and GAD2-Cre; Ai9**

(A) GAD1 (GAD67) expressing neurons are labeled with GFP. (B) Enlarged image of the adBNST at AP 0.16 mm. GAD+ neurons are distributed throughout the adBNST, particularly near the ovBNST, jcBNST, and the alBNST, with a lower concentration near the amBNST. In the vBNST, GAD+ neurons are densely located near the anterior commissure. (C) GAD2 (GAD65) expressing neurons are labeled with the red fluorescent protein (tdTomato). (D) Enlarged image of the adBNST at AP 0.19 mm. GAD2+ cells are densely located in the jcBNST. Scale Bar: 500µm (A,C), 250µm (B,D).

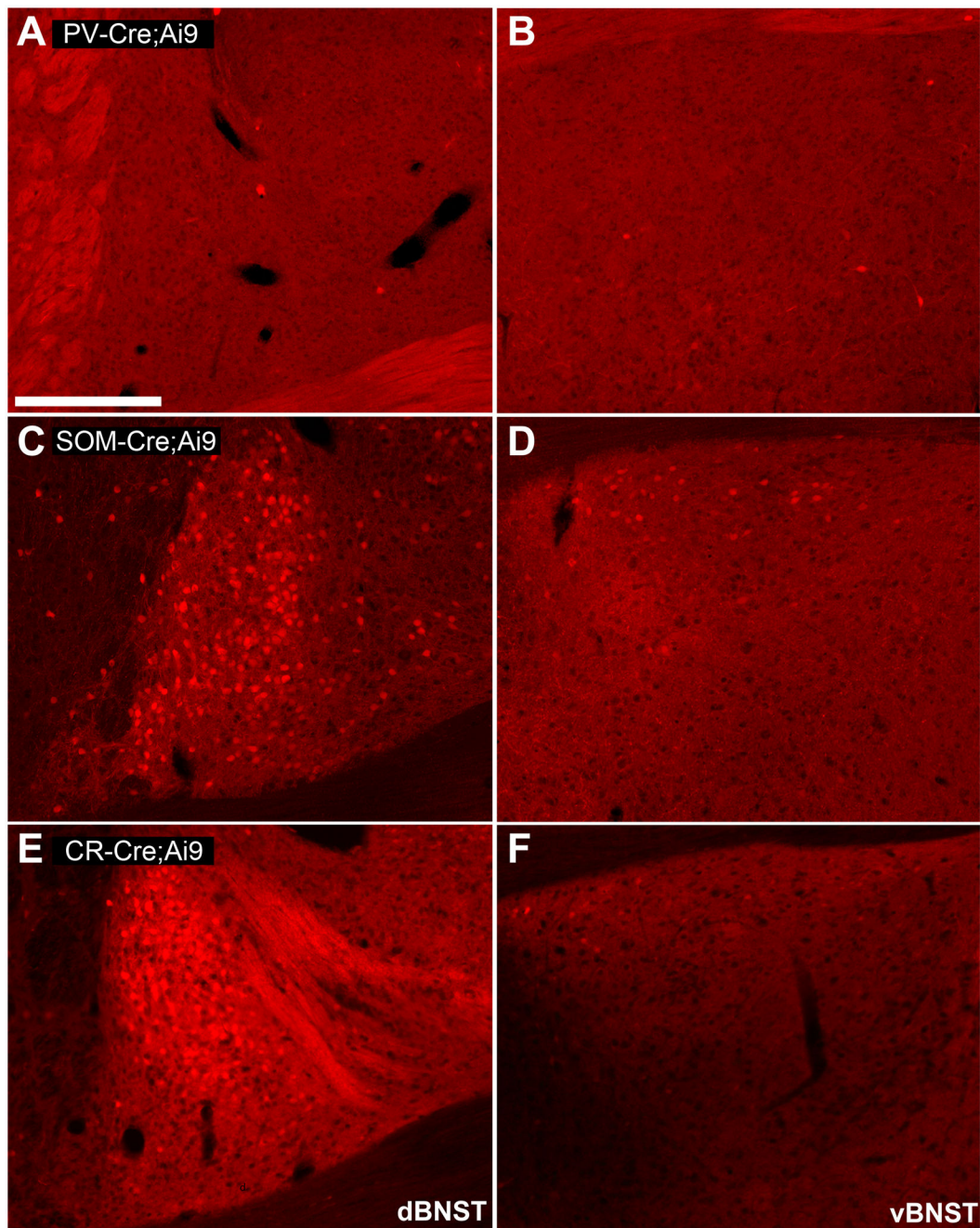


**Figure 8. Distributions of specific inhibitory cell subtypes in the bed nucleus of the stria terminalis**  
 (A–B) PV+ neurons are generally not found in the BNST of the PV-Cre; Ai 9 mouse. (C–D) A good number of SOM+ cells are distributed mostly within the anterolateral region of dorsal BNST (dBNST) of the SOM-Cre; Ai9 mouse, while SOM+ neurons found in the vBNST are sparse. (E–F) Most CR+ neurons are localized in the anterior oval BNST, with a small number of CR+ cells found in the juxtacapsular BNST (jcBNST) in the CR-Cre; Ai9 mouse. Scale bar: 250µm (A–F).

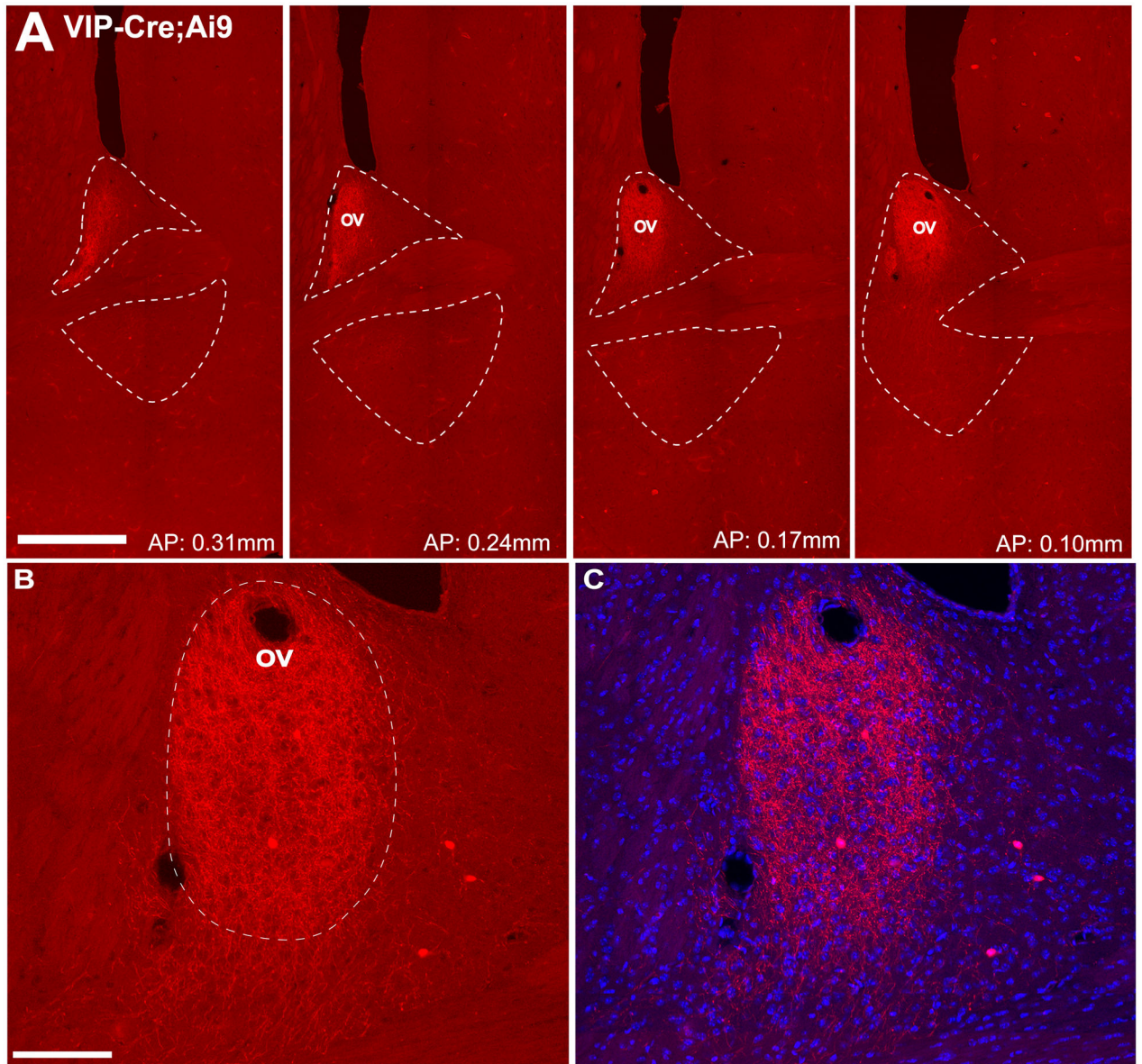


**Figure 9. VIP+ axonal plexuses are localized in the ovBNST and jcBNST**

(A) VIP+ fibers appear to run through the BNST. These fibers are abundant, and in contrast, there are very sparse VIP+ cell bodies found in adBNST. The VIP+ axonal plexuses mainly found in the ovBNST which extend towards the posterior area of the BNST. (B) Enlarged image at AP 0.17 mm. The fibers are concentrated in the ovBNST and, to a lesser extent, the jcBNST. (C) Enlarged view of the same area as (B), with DAPI staining (blue) in the background. Scale Bar: 500 $\mu$ m (A); 100 $\mu$ m (B, C).

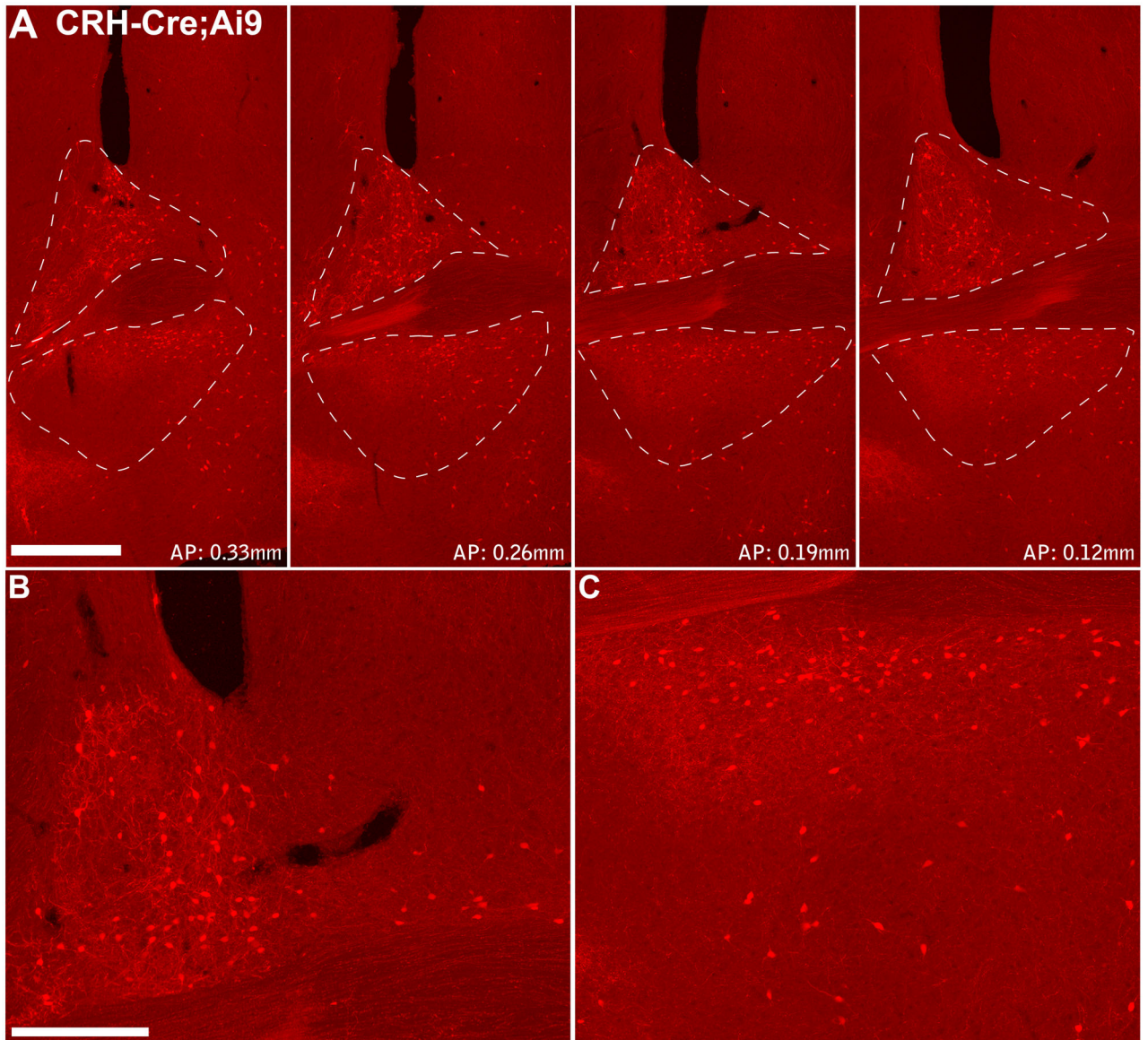


**Figure 10. Assessment of the distribution of corticotropin-releasing hormone (CRH)+ neurons in the BNST using CRH-Cre; Ai9 mouse**  
 (A) CRH+ cells are distributed throughout the adBNST and vBNST. (B) Enlarged image of the adBNST at AP 0.19 mm. (C) Enlarged image of the vBNST at AP 0.19 mm. Scale Bar: 500 $\mu$ m (A), 250 $\mu$ m (B, C).

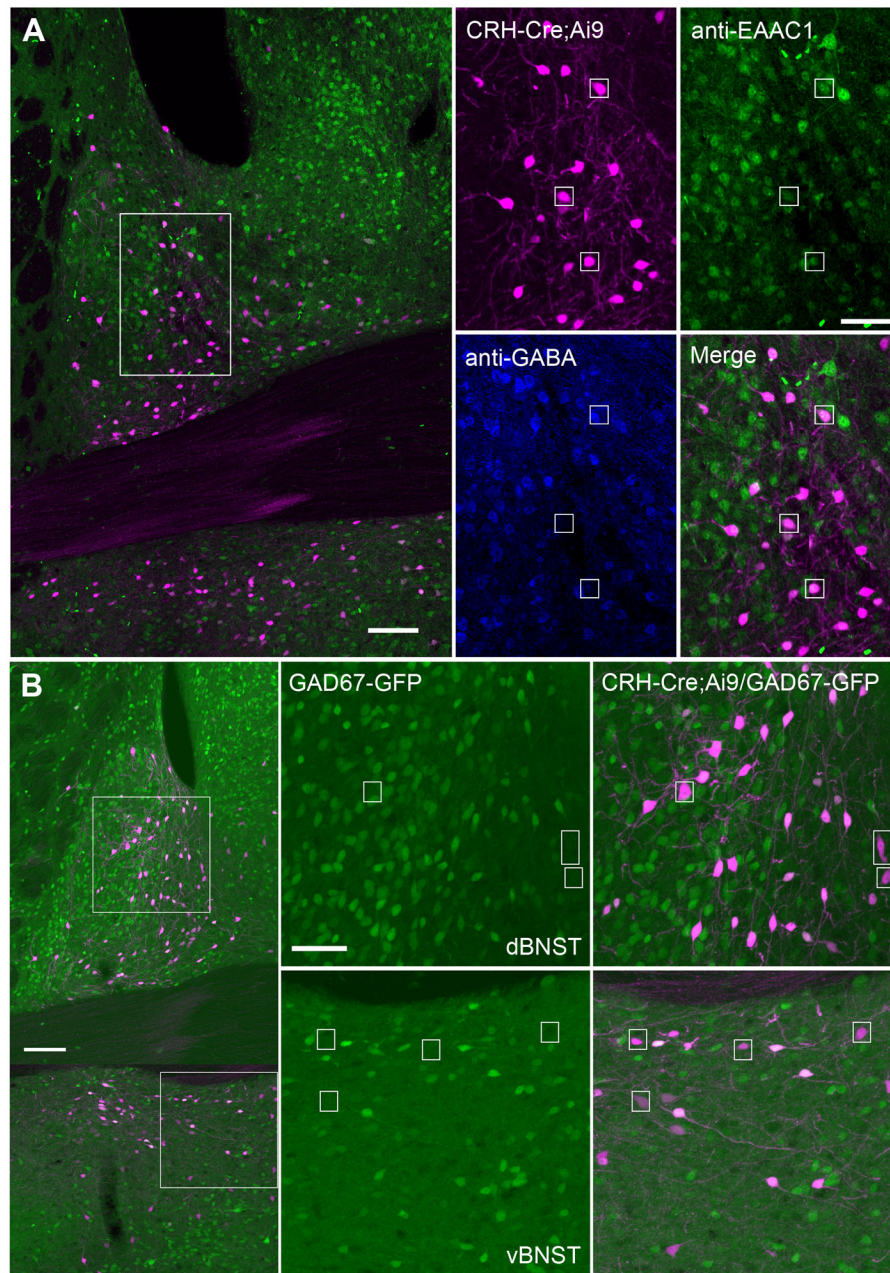


**Figure 11. CRH-expressing BNST neurons contain both GABAergic and glutamatergic neurons**  
 (A) The large panel on the left is an example image showing genetic labels of CRH-expressing neurons and immunostaining in the BNST. CRH-expressing neurons (red) were visualized in the BNST using the CRH-Cre; Ai9 mouse. EAAC1 (green) and GABA (blue) double immunohistochemistry was conducted on the CRH-Cre; Ai9 sections to identify GABAergic or glutamatergic types of CRH-expressing BNST neurons. The subtraction analysis of EAAC1+/GAD- neurons is used to infer cell types as excitatory neurons. Scale Bar: 200  $\mu$ m. The four panels on the right show the enlarged views of the white box in A, with CRH-expressing tdTomato+ neurons in red, EAAC1 staining in green, GABA staining

in blue and the overlay of all the three labels in the Merge. White squares indicate colocalization of CRH and EAAC1 but not GABA (CRH-expressing glutamatergic neurons). Scale bar = 100 $\mu$ m. (B) The large panel on the left is an example image showing genetic labels of CRH-expressing neurons and GABAergic neurons in the CRH-Cre; Ai9/GAD67-GFP mouse BNST. CRH-expressing neurons are visualized by Cre-mediated tdTomato expression (red) while GABAergic neurons (green) are visualized by GAD67-GFP expression. Colocalization of tdTomato and GFP expression indicates GABAergic CRH+ cells. Scale bar = 200  $\mu$ m. The four panels on the right show the enlarged view of the two white boxes in B, respectively. White squares indicate CRH positive but GAD67 negative neurons (CRH-expressing glutamatergic neurons). Scale bar = 100  $\mu$ m.

**Table 1**  
**Animal strains and specific cell targeting**

All mice used have a C57BL/6 congenic background. Male and female mouse numbers were balanced and four to six mice for each animal strain were used for experiments.

Animal strain	Neurochemical Target	Animal age
Camk2a-Cre; Ai9	Calcium/calmodulin-dependent protein kinase type II alpha chain	4–6 weeks old
ChAT-IRES-Cre; Ai9	Choline acetyltransferase	4–6 weeks old
CR-IRES-Cre; Ai9	Calretinin	4–6 weeks old
CRH-IRES-Cre; Ai9	Corticotropin-releasing hormone	4–6 weeks old
*CRH-IRES-Cre; Ai9/GAD67-GFP	Corticotropin-releasing hormone GAD67	4–6 weeks old
GAD2-IRES-Cre; Ai9	Glutamic acid decarboxylase 65 (GAD65)	4–6 weeks old
*GAD2-IRES-Cre; Ai9/GAD67-GFP	Glutamic acid decarboxylase 67 (GAD67); Glutamic acid decarboxylase 65 (GAD65)	4–6 weeks old
PV-IRES-Cre; Ai9	Parvalbumin	6–8 weeks old
SOM-IRES-Cre; Ai9	Somatostatin	4–6 weeks old
VGLUT2-IRES-Cre; Ai9	Vesicular glutamate transporter 2	4–6 weeks old
VIP-IRES-Cre; Ai9	Vasoactive intestinal peptide	4–6 weeks
GAD67-GFP	GAD67	4–6 weeks old

\* Double-crossed mice between Ai9/GAD67-GFP and Cre lines

Four to six mice for each animal strain were used for experiments.

**Table 2**  
**Primary antibodies used for immunochemical staining experiments**

Specific antibodies were used to detect selected chemical markers using fluorescent labeling to complement the fluorescent genetic labeling, such as tdTomato and GFP.

Antigen	Immunogen	Manufacturing details	Working dilution
NEUronal Nuclei (NeuN)	Purified cell nuclei from mice brain	EMD Millipore (Billerica, MA), mouse monoclonal, MAB377 RRID:AB_10048713	1:100
Excitatory Amino Acid Carrier 1 (EAAC1)	Synthetic peptide from the carboxy-terminus of the cloned rat EAAC1	EMD Millipore (Billerica, MA), goat polyclonal, AB1520 RRID:AB_90732	1:500
GABA	( $\gamma$ -aminobutyric acid)-BSA	Sigma-Aldrich (St. Louis, MO), rabbit polyclonal, A2052 RRID:AB_477652	1:2000
Parvalbumin (PV)	Rat muscle parvalbumin	Swant (Bellinzona, Switzerland), rabbit polyclonal, PV-28 RRID:AB_10013386	1:1000
Vasoactive Intestinal Peptide (VIP)	Porcine VIP conjugated to bovine thyroglobulin with carbodiimide	ImmunoStar (Hudson, WI), rabbit polyclonal, 20077 RRID:AB_572270	1:500
Somatostatin (SOM)	Synthetic 1–14 cyclic somatostatin conjugated to bovine thyroglobulin using carbodiimide	EMD Millipore (Billerica, MA), rat monoclonal, MAB354 RRID:AB_2255365	1:200
Calretinin (CR)	Human recombinant calretinin	Swant, rabbit polyclonal, 7699/4 RRID:AB_2313763	1:500
Calcium/calmodulin-dependent Protein Kinase II (CaMKII)	Amino acids 303-478 mapping at the c-terminus of CaMKII $\alpha$ of mouse origin	Santa Cruz Biotechnology (Santa Cruz, CA), rabbit polyclonal, sc-9035 RRID:AB_634551	1:500
Corticotrophin Releasing Hormone (CRH)	Human/rat CRH coupled to human alpha-globulins	Non-commercial, Sawchenko lab, Salk Institute, Rabbit polyclonal	1:10,000

**Table 3**  
**Average densities and percentage of specific neuron types in adBNST and vBNST**

The cell densities were measured from 25 μm coronal sections in the unit of cells/mm<sup>2</sup>. The total count of NeuN labeled cells was compared to the count of labeled neurons, and this was measured as a percentage of neurons.

	NeuN	CRH+	ChAT+	CaMKIIα+	YGLUT2+	EAACI+	EAACI+/GAD-
Average Density (cells/mm <sup>2</sup> )	165.86±12.61	13.74±1.56	0.84±0.10	25.04±2.09	0.65±0.11	35.32±2.67	23.07±2.22
Percentage of Neurons		8.28±0.23	0.50±0.04	15.10±0.95	0.39±0.05	21.29±3.1	13.91±0.39
	GAD67+/GAD65+	GAD67+	GAD65+	CR+	PV+	SOM+	VIP+
Average Density (cells/mm <sup>2</sup> )	110.28±6.35	109.07±1.88	92.25±8.93	16.94±2.53	0.21±0.13	27.93±0.85	0.70±0.15
Percentage of Neurons	66.49±2.52	65.76±0.85	55.62±0.64	10.21±0.58	0.12±0.06	16.84±0.54	0.42±0.06
	NeuN	CRH+	ChAT+	CaMKIIα+	YGLUT2+	EAACI+	EAACI+/GAD-
Average Density (cell/mm <sup>2</sup> )	139.83±14.24	18.52±1.44	2.03±0.55	12.02±1.28	1.31±0.24	49.28±5.13	40.36±4.76
Percentage of Neurons		13.24±0.42	1.45±0.24	8.60±0.54	0.93±0.07	34.53±2.68	28.86±1.60
	GAD67+/GAD65+	GAD67+	GAD65+	CR+	PV+	SOM+	VIP+
Average Density (cell/mm <sup>2</sup> )	45.14±2.73	39.67±3.75	25.66±1.29	4.96±0.83	0.44±0.31	6.10±0.95	0.24±0.08
Percentage of Neurons	32.28±1.3	28.37±0.89	18.35±0.43	3.55±0.3	0.32±0.15	4.36±0.36	0.17±0.02